Zeitschrift: Schweizerische mineralogische und petrographische Mitteilungen = Bulletin suisse de minéralogie et pétrographie

Band: 80 (2000)

Heft: 1

Artikel: Late Cretaceous-Tertiary magmatic and tectonic events in the Transhimalaya batholith (Kailas area, SW Tibet)

Autor: Miller, Christine / Schuster, Ralf / Klötzli, Urs

DOI: https://doi.org/10.5169/seals-60947

SCHWEIZ. MINERAL. PETROGR. MITT. 80, 1–20, 2000

Late Cretaceous-Tertiary magmatic and tectonic events in the Transhimalaya batholith (Kailas area, SW Tibet)

by *Christine Miller*[1], *Ralf Schuster*[2], *Urs Klötzli*[2], *Wolfgang Frank*[2] and *Bernhard Grasemann*[2]

Abstract

Major and trace element, single zircon evaporation, Rb–Sr, Sm–Nd and $^{40}Ar/^{39}Ar$ data are presented for the igneous rocks of the Andean-type plutonic belt exposed along the southern margin of the Lhasa terrane in SW Tibet. The new data (1) show that the calc-alkaline plutonism is 80 Ma older than previously thought: it started as early as 119 Ma and lasted until about 40 Ma; (2) indicate a range of eruption ages for the associated volcanic rocks of c. 119 to 38 Ma; (3) document the involvement of mantle and crustal components in the genesis of these magmatic rocks: $^{87}Sr/^{86}Sr$ initial ratios range between 0.7035 and 0.7353; (4) suggest that the intrusion of plutons occurred at crustal depths of c. 0.27–0.65 GPa; (5) confirm and extend previously published models of Cretaceous-Tertiary magmatic and tectonic events: the plutons in the northern part of the batholith had cooled to below 300 °C by 90 Ma, probably due to thrust tectonics. The postcrystallization cooling history of the Kailas pluton in the southern part is characterized by cooling to below 500 °C and exhumation to the surface between 43–23 Ma, probably due to S directed thrusting along the Gangdese thrust. Reheating around 20 Ma documents the activity of the N directed Kailas thrust system.

Keywords: SW Tibet, Transhimalaya batholith, petrology, geochronology.

Introduction

The Karakoram-Himalaya-Tibet orogenic system is the spectacular result of the collision of India and Asia and ongoing intracontinental convergence. The time of initiation of collision varies along strike of the Himalayan orogen, ranging from Early Paleocene in the west (BECK et al., 1995) to mid-Eocene in the east (DEWEY et al., 1988). Much of the complex tectonic history is recorded in rocks along the Indus-Tsangpo Suture zone (IYS) that marks the closure of the Tethyan ocean. The calc-alkaline magmatic rocks exposed along the southern margin of the Lhasa terrane in SW Tibet are a part of the Transhimalaya magmatic belt (THB) which extends almost continuously north of the Himalaya over a distance of c. 3000 km from Pakistan to Burma (Fig. 1). Dioritic, granodioritic and granitic plutons predominate in this Andean-type magmatic system (e. g. DEBON et al., 1986). Together with volcanic rocks they were emplaced along the southern continental margin of Eurasia as a consequence of the subduction of the Neotethyan oceanic plate during the Cretaceous and Paleocene (e. g. GANSSER, 1964; HONEGGER et al., 1982; DEWEY et al., 1988). Studies of such volcanic-plutonic systems may provide information about the geochemistry and timing of magmatic activity and continental-margin tectonics in the southern part of Eurasia during the convergence and collision with the Indian plate. Previous studies have concentrated on the Kohistan arc-batholith (e. g. PETTERSON and WINDLEY, 1985; 1991) and on the Karakoram batholith (e. g. CRAWFORD and SEARLE, 1992) in Pakistan, on the Ladakh intrusives (e. g. HONEGGER et al., 1982; SCHÄRER et al., 1984a) and on the Lhasa-Xigaze sector (e. g. SCHÄRER et al., 1984b). In these sectors (Fig. 1), published isotopic data have established an intrusive age span of c. 103–30 Ma. In contrast, in SW Tibet, geochronological data

[1] Institut für Mineralogie und Petrographie, University of Innsbruck, Innrain 52, A-6020 Innsbruck, Austria. <Christine.Miller@uibk.ac.at>

[2] Institut für Geologie, Althanstraße 14, University of Vienna, A-1090 Wien, Austria.

available so far have yielded a surprisingly young age of c. 39 Ma for the subduction-related magmatic activity (HONEGGER et al., 1982). Based on new geochronological and geochemical data of plutonic and volcanic rocks, this paper shows that the Xungba-Kailas segment of the THB in southwest Tibet has experienced a complex tectonic and magmatic history, which is 80 Ma older than previously thought.

Regional geology

The Tibetan plateau, between the Kun Lun Shan and the Himalayas, is the largest and highest plateau on Earth. It formed in response to the India-Asia collision and consists of terranes accreted successively to Eurasia since the Early Paleozoic. The Lhasa Block, the southernmost of these continental fragments, accreted to Asia along the Banggong Suture during the Late Jurassic (e. g. DEWEY et al., 1988). It formed the southern Eurasian plate margin during the Cretaceous. Along the length of the Himalaya, the junction between the Indian and Asian plates is marked by the IYS and its ophiolite remnants.

The composite Transhimalaya plutonic complex is emplaced immediately north of the IYS (Fig. 2) where it intrudes the folded sediments (c. 1500 m) of the Middle to Upper Cretaceous Takena Formation (BURG et al., 1983). There is no evidence of basement gneisses. Rock types range from hornblende gabbro to granite, but the most abundant lithologies are hornblende quartz diorites and granodiorites. Mafic enclaves are common in hornblende bearing granitoids. The northern limit of the batholith is equivocal. In this study the belt is extended to include the granitic rocks south of Xungba and south of Bongba, about 130 km north of the IYS, on the basis of their age and geochemical similarities with rocks exposed in the Kailas area. About 40 km W of Mt. Kailas, the Moincer Formation covers an area of c. 350 km^2 (Fig. 2). It includes the youngest marine sediments (c. 53 Ma) found along the IYS in SW Tibet, i. e. Eocene limestones with *Nummulites sp.* as well as alluvial fan, fluviatile and lacustrine deposits containing Eocene coal-beds. These sediments unconformably onlap the eroded surface of the THB batholith and the Takena Formation north of the IYS. They are transgressed, in turn, by deposits of the Kailas Molasse.

In the Kailas area wall-rock contacts are not exposed: S of Mt Kailas, the southern side of the batholith is unconformably transgressed by the alluvial fan and deltaic deposits of the Kailas Molasse (Fig. 2), left behind by a river that entered this post-Eocene intramontane molasse basin

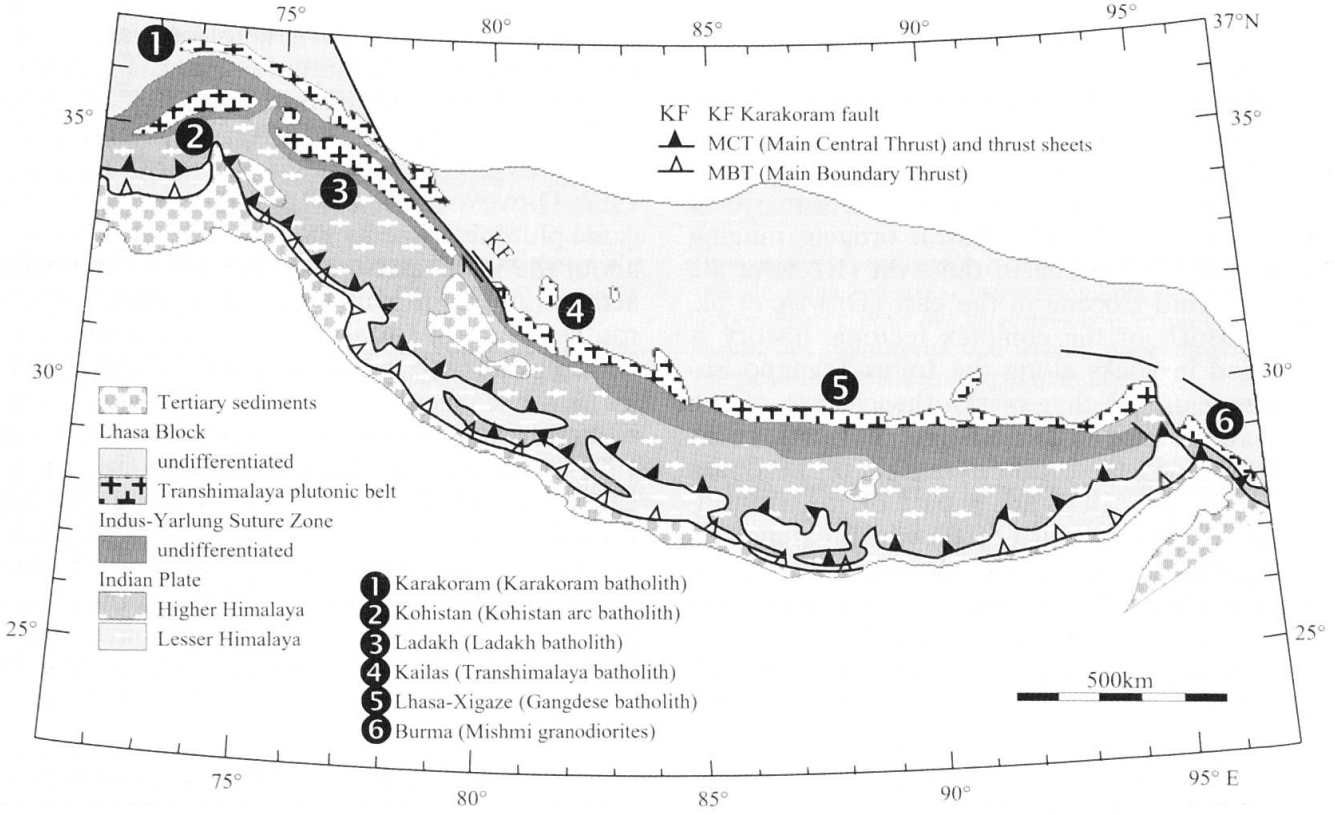

Fig. 1 Tectonic sketch map showing the position of different segments within the Transhimalaya magmatic belt.

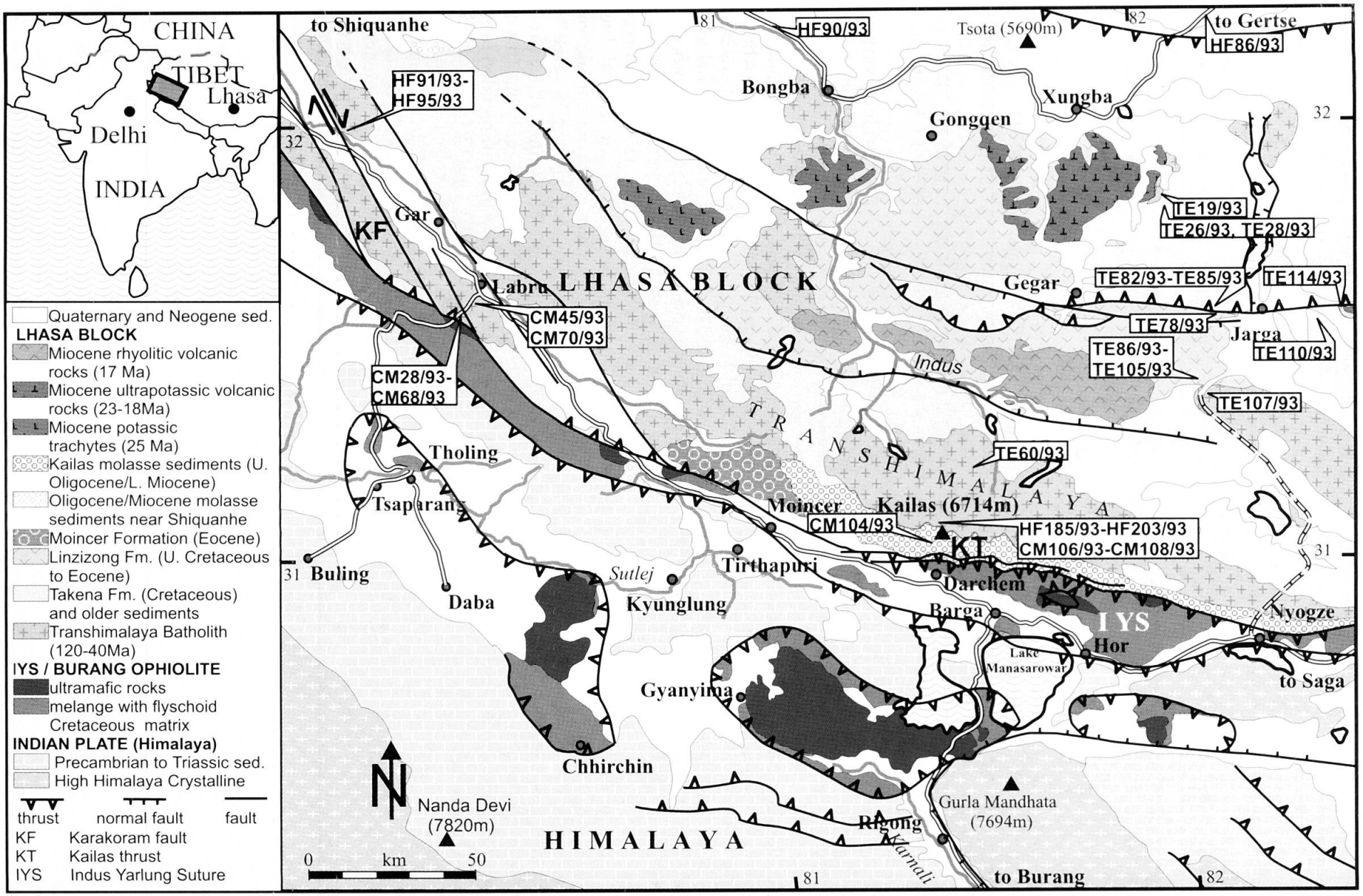

Fig. 2 Simplified geological map of the Lhasa block in SW Tibet with sample locations. Compiled from field mapping, SPOT and Landsat MSS images, and the geological map 1: 1.500.000 of Qinghai-Xizang (Tibet) plateau and adjacent areas (Chinese Academy of Earth Sciences, Beijing, 1983).

from the north (HEIM and GANSSER, 1939). *Unionidae* bivalves in marly layers of the middle part of this 2000 m thick formation indicate an Upper Oligocene/Lower Miocene (c. 23 Ma) age and a non-marine, possibly brackish environment for the deposition of the Kailas Molasse sediments (SCHUSTER et al., 1997).

Based on geologic mapping and geochronological analysis, YIN et al. (1999) proposed a three stage kinematic model for the Tertiary tectonic development of the Kailas area: *Stage 1 (50–30 Ma):* initiation of the south directed Gangdese thrust within the THB (= Gangdese igneous belt). *Stage 2 (30–20 Ma):* movement on the Gangdese thrust, exhumation and cooling of the Gangdese batholith in the hanging wall of the thrust. The lower Kailas conglomerates with south-directed paleocurrent indicators were deposited synchronous with thrusting. *Stage 3 (20–4 Ma):* movement of the north-directed Kailas thrust system, an equivalent of the Great Counter thrust (HEIM and GANSSER, 1939). The upper part of the Kailas conglomerates is derived from the hanging wall and characterized by northward paleocurrent indicators. Our data support the model of YIN et al. (1999), but extend the magmatic and tectonic history of the THB back to 120 Ma.

Petrography

A set of 101 samples was collected over 100 km along strike, ranging from Bamba in the N to Gar in the NW to the Kailas pluton in the SW (Fig. 2). Previous work has been reconnaissance in nature with limited geochemical and isotopic data (HEIM and GANSSER, 1939; GANSSER, 1964; HONEGGER et al., 1982).

CALC-ALKALINE PLUTONIC COMPLEXES

(1) Kailas – In the Kailas area the rock types range from hornblende gabbro to granite, the dominant lithologies being quartz monzodiorite and granodiorite (e. g. HF197/93) with abundant mafic enclaves. Tourmaline ± garnet bearing pegmatites and aplitic dikes are common and mark the end of magmatic activity in the Kailas area.

(2) Labru – In this pluton southwest of Labru a hornblende gabbro net-vein complex is exposed at the lowest topographic levels (c. 4200 m), indicative of mingling of coexisting mafic and silicic magmas. Upwards in the section hornblende-bearing quartz diorites, quartz monzodiorites and granodiorites with abundant mafic enclaves predominate. Angular blocks of quartzite and fine-grained schists are found near the top of the exposure (c. 5800 m). Porphyritic rhyolitic dikes (CM28/93, CM 60/93) cut the granitic rocks, indicating emplacement at high levels. The lower part of this complex is extensively fractured and rests upon a > 200 m thick, north-dipping mylonitic shear zone. In the south, a north-dipping fault juxtaposes the THB plutonic rocks over the IYS. The relationship between the mylonitic shear zone and this thrust is unknown at present.

(3) Plutons N of the Transhimalaya range – Samples have been investigated from a number of plutons exposed N of Mt. Kailas. At all sample localities, E Bamba (Hb-granodiorite HF86/93), S Xungba (Hb-granodiorite TE19/93; granitic dike TE129/93), W Gegyai (Hb-qtz-diorite HF90/93) and Sengdoi (leucogranite TE60/93), these igneous rocks intrude the Cretaceous Takena formation (Fig. 2).

The granitic rocks of the THB exhibit a variety of microfabrics ranging from hypidiomorphic equigranular to porphyritic. Al-poor salitic clinopyroxenes may occur in the cores of large hornblende grains in granodiorites and mafic enclaves. In addition to clinopyroxene, hypersthene is present in mafic enclave CM108/93 where it is partly replaced by cummingtonite. Magmatic amphiboles fall within the calcic magnesio-hornblende field (classification scheme of LEAKE, 1978). Accessory minerals include epidote, magnetite, apatite, sphene, allanite and zircon. The epidotes form intergrowths with amphibole or biotite and range from Ps_{24} to Ps_{26} [$Ps = Fe^{3+}/(Fe^{3+} + Al)$]. This is within the chemical range proposed by TULLOCH (1976) for primary magmatic epidote in granitic rocks. In the hornblende-granodiorite samples HF197/93 and TE19/93 zircon crystals are euhedral, clear and colourless without visible cores or overgrowths. The zircon populations have morphologic characteristics typical for calc-alkaline granitoids with maxima in fields S24 (HF197/93), D and J5 (TE19/93) of the zircon classification diagram (PUPIN and TURCO, 1972). Secondary minerals include sericite, chlorite and/or prehnite.

Hornblende gabbros and hornblende-biotite diorites with equigranular or porphyritic microfabric and fine to medium-grained mafic enclaves are associated with the Hb-granitoids. In more intermediate host rocks (55–60% SiO_2), the enclaves consist of clinopyroxene-hornblende-plagioclase-magnetite, whereas more felsic granitoids (> 60% SiO_2) contain hornblende-plagioclase-magnetite inclusions.

GAR SYENITIC COMPLEX

This complex crops out in the Gar valley, about 70 km SE Shiquanhe and just N of the Karakorum Fault. Medium-grained syenites (HF91/93) are the predominant lithology. They are cut by mafic and trachytic (HF95/93) dikes. The syenites contain quartz, K-feldpar, plagioclase, salitic clinopyroxene, amphibole (potassian-edenitic to potassian-ferro-edenitic hornblende) and biotite rich in F (c. 3 wt%) and Cl (0.5 wt%). K-feldpar has a mean composition of $Or_{75}Ab_{25}An_1$, the plagioclase is zoned from $Ab_{47}An_{52}Or_1$ (core) to $Ab_{61}An_{36}Or_3$ (rim). Accessory minerals are sphene (c. 3.6 wt% Al_2O_3), ilmenite (c. 10 wt% MnO), magnetite, apatite, zircon and fluorite.

CALC-ALKALINE VOLCANIC ROCKS

At the base of the Cretaceous Takena Formation andesitic lavas are interbedded with terrestrial clastic sediments and crosscut by rhyolitic and andesitic dikes. Higher up in the sequence, massive andesitic lava flows (TE82/93, TE110/93), up to several tens of meters thick, are interbedded with tuffaceous sediments. A later cycle is made up of marine marls and limestones containing a fauna of Aptian to Albian *naticide* bivalves and foraminifera (SCHUSTER et al., 1997), tuffaceous layers and volcanoclastic olistostromes. The top of the Takena Formation consists of rhyolitic ignimbrites, tuffs (TE28/93) and tuffaceous sandstones with subordinate intercalations of marine sediments. Along the line Gegar–Jarga (Fig. 2) a north-dipping thrust juxtaposes the Takena Formation over rocks of the Upper Cretaceous to Eocene Linzizong Formation. In the section west of Jarga the basal unit of the Linzizong Formation consists of volcanoclastic rocks with intercalations of marls. This sequence is crosscut by andesitic dikes (TE69/93) and capped by andesitic lava flows (TE71/93, TE73/93) and pyroclastic rocks. The middle part is formed by about 400 m of dacitic and rhyolitic ignimbrites (TE78/93, TE114/93) and tuffs. The uppermost 500 m of the Linzizong Formation consist of tuffaceous sand- and siltstones.

The mafic THB volcanic rocks and basaltic andesites are plagioclase-phyric. In addition, phenocrysts of clinopyroxene ($Wo_{37-40}En_{46-47}Fs_{12-16}$) ± olivine may be present. The intermediate volcanic rocks contain a phenocryst assemblage of plagioclase + titanian-(± ferroan)-pargasitic hornblende ± biotite. Plagioclase phenocrysts in the THB andesitic rocks are commonly zoned (cores: An_{58-51}, rims: An_{55-34}). In addition, they may contain highly calcic (An_{85-88}) xenocrystic cores. The felsic volcanic rocks are porphyritic or vitrophyric with corroded quartz + plagioclase + alkalifeldspar + biotite phenocrysts. Glassy samples often contain flattened pumice fragments with eutaxitic microfabrics characteristic of welded tuffs. The Labru rhyolitic dikes contain quartz + plagioclase + alkalifeldspar + biotite + muscovite as phenocrysts. All volcanic rocks contain apatite and magnetite with highly variable TiO_2 contents (2.6–20.3 wt%). Zircon is ubiquitous in silicic volcanic rocks. Alteration phenomena are common and include sericitization of feldspars, replacement of olivine by iddingsite and/or carbonate, opacitization of hornblende and biotite, and replacement of clinopyroxene, hornblende and biotite by chlorite.

THERMOBAROMETRIC ESTIMATES

Diorite and granodiorites of the THB contain the assemblage hornblende + biotite + plagioclase + K-feldspar + quartz + sphene + Fe–Ti oxide required for hornblende barometric estimates using the calibration of SCHMIDT (1992). These pressures range from 0.27 (Kailas) to 0.65 GPa (HF90/93; Gegyai) for different plutons, corresponding to a crystallization depth of about 9.8–23.6 km. Epidote with textural characteristics suggestive of a magmatic origin is present only in plutons emplaced at pressures of 0.36 GPa or greater. Temperatures calculated with the geothermometer of BLUNDY and HOLLAND (1990) are indistinguishable for mafic enclaves and host granitoids and suggest equilibration at conditions of c. 700–780 °C. Temperature estimates based on zircon solubility data (WATSON and HARRISON, 1983) are in the range of 726–815 °C for THB Hb-granitoids and mafic enclaves. Zircon solubility temperatures calculated for the THB silicic volcanic rocks are in the range of 736–848 °C. The A-type syenites yielded clearly higher temperatures of 875–930 °C.

Major, trace element and isotope geochemistry

Major, trace and rare-earth element (REE) data for selected THB lithologies are presented in table 1. Analytical methods are given in MILLER et al. (1999).

The mostly medium- to high-K *calc-alkaline plutonic rocks* cover a wide range in SiO_2 composition (51.9–73.6%). Hornblende-gabbros, granodiorites and granites have trace element signatures typical for calc-alkaline magmas at active

Tab. 1 Major (wt%), trace element and REE (ppm) concentrations of magmatic rocks, Transhimalaya batholith, SW Tibet.

Sample no.:	HF197/93	HF191/93	CM108/93	CM070/93	CM045/93	TE073/93	TE082/93	TE086/93	TE059/93	TE110/93	HF092/93	HF095/93
Lithology	Hb-gr	Bio-gr	ME	Hb-gabbro	Hb-gr	basalt	basalt	andesite	dacite	andesite	syenite	trachyte
Location	Kailas	Kailas	Kailas	Labru	Labru	S Bongba	S Bongba	S Jarga	NE Indus	E Jarga	Gar	Gar
SiO_2	61.89	71.95	54.93	46.94	65.67	48.24	50.35	61.09	68.70	54.58	59.94	62.32
TiO_2	0.68	0.24	0.91	1.48	0.50	1.50	1.13	0.87	0.29	1.10	0.52	0.63
Al_2O_3	16.11	14.00	18.46	16.63	15.58	15.49	18.09	15.33	16.06	18.29	18.71	17.92
Fe_2O_3	5.18	1.44	7.22	12.00	3.70	10.59	8.93	5.85	2.15	8.98	4.55	4.29
MnO	0.12	0.05	0.14	0.18	0.09	0.17	0.17	0.10	0.06	0.23	0.15	0.15
MgO	1.89	0.56	3.64	7.30	1.53	4.97	5.05	2.43	0.59	2.77	0.97	1.02
CaO	4.72	1.65	6.22	8.63	2.52	11.92	10.04	4.97	2.06	8.04	2.50	2.20
Na_2O	3.72	3.52	4.08	2.91	3.37	3.16	3.63	3.47	2.95	3.28	4.39	3.96
K_2O	3.78	4.90	2.86	1.89	4.89	1.47	0.56	4.15	3.88	0.64	6.48	7.27
P_2O_5	0.23	0.09	0.38	0.35	0.31	0.49	0.36	0.54	0.13	0.27	0.24	0.17
LOI	0.76	0.66	0.66	1.97	0.76	1.74	2.14	1.39	3.04	1.26	0.58	0.70
Total	99.08	99.06	99.50	100.28	98.92	99.74	100.45	100.19	99.91	99.44	99.03	100.63
F	560	870									2040	1060
Cl	170	40									490	250
Be	2.5	9.9	2.4	1.2	6.6	1.3	0.9	3.1	3.5	0.6	17.7	11.5
Sc	10	5	14	28	6	19	19	15	11	24	5	6
V	116	23	151	391	67	213	235	152	29	120	32	23
Cr	22	5	36	12	36	67	67	94	11	17	12	5
Co	13	3	9	6	7	40	44	10	3	5	5	4
Ni	17	3	23	25	17	38	22	33	7	8	6	2
Cu	28	4	44	97	21	43	49	33	6	14	18	17
Zn	50	31	87	115	50	90	87	67	41	107	67	98
Ga	19	20	21	20	19	19	19	18	18	20	21	20
Rb	156	345	98	89	221	30	11	190	209	17	385	309
Sr	524	218	698	573	601	770	742	1147	403	344	399	268
Y	19	12	18	20	11	17	19	23	14	27	46	42
Zr	183	140	176	148	219	116	127	220	135	97	621	529
Nb	10	15	11	5	19	5	11	9	10	4	56	44
Ba	674	549	727	539	1035	517	220	1711	908	205	382	445
Hf	4.7	4.3	5.0	4.3	6.0	3.3	3.5	n. d.	4.0	n. d.	14	12.3
Ta	0.97	2.3	0.7	0.4	1.5	0.3	0.4	n. d.	1.4	n. d.	3.8	2.8
Pb	17	57	33	10	87	9	141	46	39	9	22	35
Th	24	34	12	6	61	5.64	4	24	19	5	75	55.6
U	4	10	1	1	9	1	< 1	< 2	5	4	12	7
La	37	40	37	15	52	29	22	53	37	10	100	77
Ce	74	72	72	36	107	60	45	109	76	23	193	160
Pr	8	7	8	5	12	7	6	13	8	3	18	16
Nd	30	22	29	21	39	30	24	50	30	14	63	56
Sm	6	4	5	5	6	6	5	9	5	4	11	10
Eu	1.4	0.8	1.6	1.5	1.2	1.9	1.5	2.3	1.0	1.4	1.3	1.6
Gd	4	3	4	4	4	5	4	6	4	4	9	9
Tb	0.6	0.4	0.6	0.7	0.5	0.7	0.6	0.8	0.5	0.7	1.3	1.3
Dy	3.5	2.2	3.5	3.7	2.1	3.3	3.6	3.8	2.7	3.9	7.2	7.8
Ho	0.77	0.44	0.69	0.75	0.38	0.71	0.78	0.68	0.51	0.92	1.7	1.67
Er	1.9	1.2	1.6	1.9	1.0	1.6	2.0	1.8	1.4	2.4	4.3	4.3
Tm	0.28	0.17	0.27	0.29	0.12	0.24	0.26	0.24	0.20	0.38	0.74	0.71
Yb	2.0	1.3	1.8	2.0	0.8	1.5	1.9	1.6	1.4	2.5	5.3	4.9
Lu	0.32	0.20	0.28	0.31	0.12	0.24	0.28	0.26	0.25	0.42	0.88	0.77

Bio = biotite; gr = granitoid; Hb = hornblende; ME = mafic enclave; n. d. = not determined.

continental margins, such as enrichments in Rb, Ba, Th, K, Ce and Sm relative to Nb, Ta, Zr, Y and Yb (Figs 3a–b). The THB hornblende-granodiorites have Ce_N/Yb_N ratios in the range of 9–34 and negative Eu anomalies (Eu/Eu* = 0.78–0.86). A further significant feature are the low values of Y

Tab. 2 Sr and Nd isotopic data for plutonic and volcanic rocks from the Transhimalaya batholith, SW Tibet.

Sample no.:	Locality	Lithology	Age*	Rb (ppm)	Sr (ppm)	$^{87}Rb/^{86}Sr$	$^{87}Sr/^{86}Sr \pm 2\sigma$	$^{87}Sr/^{86}Sr(i)$	Sm (ppm)	Nd (ppm)	$^{143}Sm/^{144}Nd$	$^{143}Nd/^{144}Nd \pm 2\sigma$	$\varepsilon(t)Nd$	$T(Nd)_{DM}$ Ga
PLUTONIC ROCKS														
HF086/93	E Bamba	Bio-granite	120	114.5	164.3	2.018	0.71220 ± 9	0.70876						
HF090/93	W Gegyai	Hb-granodiorite	120	86.5	291.1	0.858	0.71556 ± 7	0.71410						
HF185/93	W Kailas	Hb-granodiorite	120	156.0	396.6	1.138	0.70637 ± 15	0.70443						
HF187/93	W Kailas	mafic enclave	120	136.7	443.7	0.891	0.70632 ± 9	0.70480	5.40	32.90	0.099	0.512516 ± 7	–0.9	0.74
HF191/93	NW Kailas	Bio-granite	120	342.7	212.1	4.682	0.71677 ± 8	0.70878	3.67	23.99	0.092	0.512251 ± 6	–5.9	1.01
HF193/93	NW Kailas	Hb-granite	120	246.5	312.2	2.286	0.70894 ± 10	0.70504						
HF197/93	NW Kailas	Hb-granodiorite	120	154.3	520.3	0.858	0.70638 ± 4	0.70492	5.40	30.32	0.108	0.512528 ± 7	–0.8	0.78
HF198/93	NW Kailas	leucogranite	120	370.5	176.6	6.079	0.72007 ± 06	0.70970						
HF200/93	NW Kailas	Bio-granite	120	266.8	201.3	3.839	0.71540 ± 10	0.70885						
HF202/93	E Kailas	Hb-granodiorite	120	162.4	453.9	1.036	0.70634 ± 4	0.70457						
HF203/93	E Kailas	mafic enclave	120	140.9	477.6	0.854	0.70630 ± 6	0.70484						
CM106/93	E Kailas	Hb-granodiorite	120	148.1	515.5	0.831	0.70653 ± 7	0.70511						
CM108/93	E Kailas	mafic enclave	120	93.6	689.9	0.393	0.70807 ± 13	0.70740	4.35	30.36	0.087	0.512484 ± 5	–1.3	0.71
HF189/93	NW Kailas	aplitic dike	40	327.4	178.9	5.301	0.71433 ± 5	0.71132						
HF194/93	NW Kailas	aplitic dike	40	499.7	12.8	113.842	0.77363 ± 19	0.70895						
HF196/93	NW Kailas	aplitic dike	40	335.2	31.8	30.594	0.73540 ± 6	0.71902						
CM045/93	S Labru	Hb-granodiorite	120	21.2	59.6	1.030	0.71201 ± 7	0.71045						
CM070/93	S Labru	Hb-gabbro	120	81.0	560.2	0.418	0.70526 ± 9	0.70455	5.11	21.38	0.145	0.512624 ± 6	0.5	0.97
TE060/93	Indus source	leucogranite	40	177.2	18.1	28.325	0.72688 ± 14	0.71079						
TE019/93	SE Xungba	Hb-granodiorite	116	210.6	275.5	2.213	0.70986 ± 5	0.70608	6.94	40.64	0.103	0.512491 ± 6	–1.5	0.80
TE107/93	S Jarga	Hb-granodiorite	120	327.4	410.5	1.520	0.70634 ± 11	0.70375						
HF091/93	SE Gar	syenite	64	392.4	257.5	4.410	0.70756 ± 5	0.70355	9.16	52.72	0.105	0.512620 ± 6	0.4	0.64
HF092/93	SE Gar	syenite	64	405.0	356.6	3.287	0.70657 ± 7	0.70358						
HF095/93	SE Gar	trachyte	64	307.3	262.3	3.390	0.70662 ± 6	0.70354	10.17	58.82	0.104	0.512633 ± 6	0.7	0.62
VOLCANIC ROCKS														
TE026/93	SSE Xungba	basalt (TF)	120	32.2	437.3	0.213	0.70819 ± 5	0.70783	2.90	9.47	0.185	0.512228 ± 9	–7.8	3.60
TE082/93	W Jarga	basaltic andesite (TF)	120	10.8	738.8	0.043	0.70554 ± 5	0.70547	5.10	24.79	0.124	0.512593 ± 6	0.2	0.81
TE086/93	SW Jarga	andesite (LZ)	55	182.6	1154.4	0.458	0.70846 ± 6	0.70810	9.07	50.08	0.109	0.512292 ± 8	–6.1	1.10
TE087/93	SW Jarga	dacite (LZ)	45	148.0	518.5	0.826	0.70630 ± 8	0.70577						
TE091/93	SW Jarga	andesite (LZ)	55	139.9	611.1	0.663	0.70529 ± 5	0.70477						
TE092/93	SW Jarga	andesite (LZ)	55	151.4	581.0	0.754	0.70657 ± 6	0.70598						
TE105/93	SW Jarga	rhyolite (LZ)	55	196.5	49.3	11.550	0.71358 ± 6	0.70455						
TE110/93	E Jarga	andesite (LZ)	55	15.3	337.0	0.132	0.70623 ± 5	0.70613						
TE114/93	E Jarga	andesite (LZ)	55	176.9	473.7	1.081	0.70610 ± 5	0.70525	5.10	26.90	0.115	0.512482 ± 8	–2.5	0.90
CM048/93	SW Labru	dacite dike	37	167.0	326.0	1.500	0.70925 ± 3	0.70846						
CM051/93	SW Labru	dacite dike	37	184.0	603.0	0.893	0.70924 ± 3	0.70877						
CM028/93	SW Labru	rhyolite dike	37	189.3	195.3	2.812	0.73194 ± 6	0.73046						
CM060/93	SW Labru	rhyolite dike	37	225.0	265.0	2.463	0.73660 ± 8	0.73530						
CM104/93	Kailas Molasse	rhyolite		140.2	11.5	35.438	0.73406 ± 19							

* For volcanic rocks Ar–Ar ages were used to determine Io and $\varepsilon(t)Nd$. LZ = Linzizong Formation; TF = Takena Formation.

(< 0.54) and Yb (< 0.36) relative to ocean ridge granites (PEARCE et al., 1984).

The metaluminous *syenites* and trachytic dikes plot in the within-plate granite field of PEARCE et al. (1984) (Fig. 3d) and in the A-type granitoid fields (Figs 3e–f) of WHALEN et al. (1987). They are characterized by high $K_2O + Na_2O$ (11–12 %), K_2O/Na_2O (1.4–2.3), Zr (530–1045 ppm), F

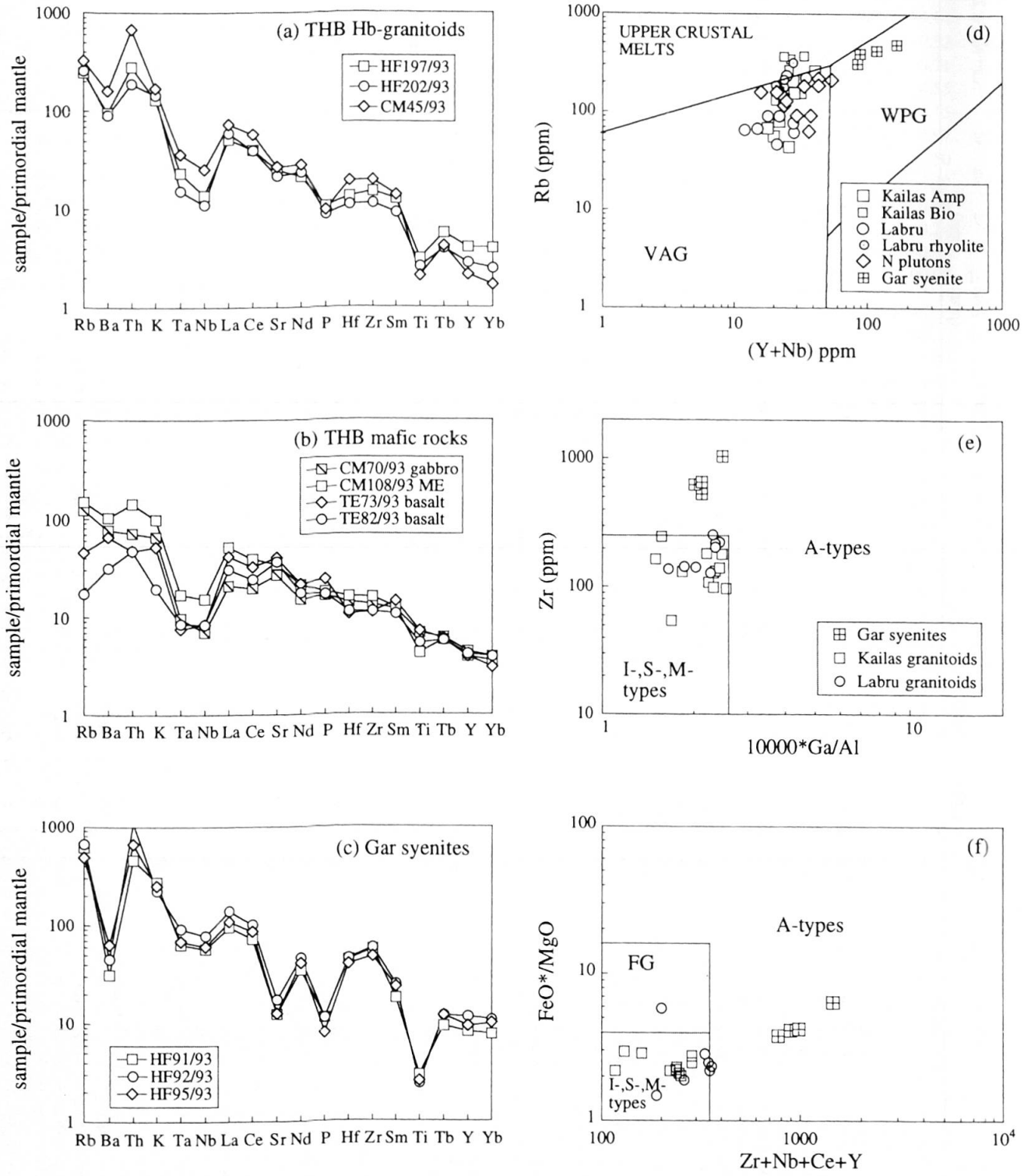

Fig. 3 Trace element variation diagrams for intrusive and volcanic rocks of the Transhimalaya batholith in SW Tibet: (a) metaluminous Hb-granitoids, (b) THB mafic rocks, (c) Gar alkaline syenites and trachyte. Normalization factors are from SUN and MCDONOUGH (1989). (d) Rb vs (Nb + Y) plot for granitic rocks from SW Tibet. Field boundaries from PEARCE et al. (1984). VAG = volcanic arc granites, WPG = within-plate granites. (e) Granitic rocks plotted on the Ga/Al vs Zr (ppm) and (f) Zr + Nb + Ce + Y (ppm) vs FeO*/MgO discriminant diagrams from WHALEN et al. (1987). FG = field for fractionated I-type granitoids.

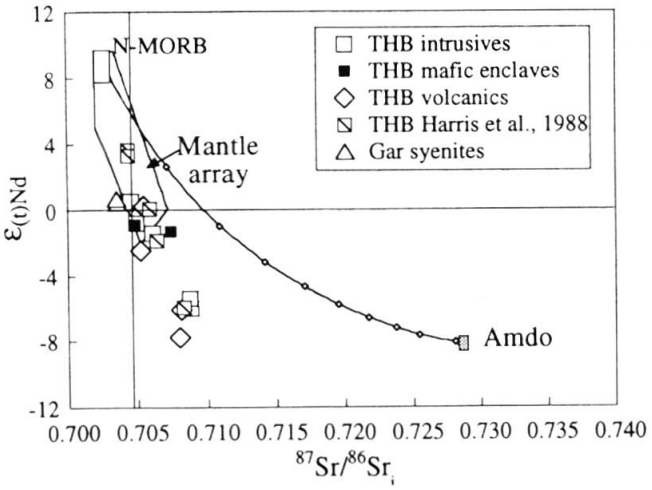

Fig. 4 εNd versus initial $^{87}Sr/^{86}Sr$ data of the THB plutonic and volcanic rocks from SW Tibet. In addition, Gangdese plutonic rocks from the Lhasa transect (HARRIS et al., 1988) are shown. Mixing calculations illustrate the effects of bulk assimilation of continental crust. The basalt composition used in modeling has $^{87}Sr/^{86}Sr$ = 0.7027, $^{143}Nd/^{144}Nd$ = 0.51294, Sr = 90 ppm, Nd = 7.3 ppm. The crustal component is Amdo orthogneiss (HARRIS et al., 1988). Points on mixing curves are at 10% intervals.

(1060–2040 ppm), Cl (250–490 ppm), relatively high Y (40–65 ppm), Nb (43–104 ppm), REE (except Eu) and low Y/Nb ratios (0.62–0.95) compared to the I-type hornblende granitoids. The normalized trace element patterns (Fig. 3c) are characterized by peaks at Th and Zr, a small Nb–Ta trough and distinct negative anomalies for Ba, Sr, P and Ti. All rocks are enriched in light REE with Ce_N/Yb_N = 8–9, and show pronounced negative Eu anomalies (Eu/Eu* = 0.42–0.83).

The analyzed THB *volcanic rocks* display a wide variation in SiO_2 (48–76%). Most samples have > 52% SiO_2, low MgO (< 6%) and high Al_2O_3 (15–19%), which underlines the evolved nature of these rocks. They are predominantely high-K calc-alkaline to shoshonitic in character. The analyzed basalts are LREE enriched (Ce_N/Yb_N = 6–10), without Eu-anomalies. Figure 3b illustrates a typical arc-like trace element signature with enriched large ion lithophile elements (Rb, Ba, K, Th, La, Sr) and depleted high field strength elements (Nb, Ta, Ti). With Ba/Nb > 30 they can be classified as orogenic according to the definition of GILL (1981).

The Sr and Nd isotopic data are presented in table 2. The initial $^{87}Sr/^{86}Sr$ ratios of the THB plutonic and volcanic rocks span a large range, from 0.7035–0.7366, as do the initial εNd values (–7.8 to +0.5). They show the usual negative correlation in the conventional Nd–Sr isotope diagram (Fig. 4). The GSC syenites and trachytes are characterized by low $^{87}Sr/^{86}Sr$ initial ratios (≈ 0.7034) and by positive initial εNd values in the range of 0.4 to 0.7.

Timing of magmatic activity

PLUTONIC COMPLEXES

Table 3 lists the new geochronological data on the SW Tibetan segment of the THB. The analytical details are presented in MILLER et al. (1999) and in the appendix. HONEGGER et al. (1982) published a well defined Rb–Sr whole rock isochron of 38.8 ± 3.3 Ma (initial $^{87}Sr/^{86}Sr$ ratio = 0.70609) from the Kailas area. This isochron was based on small (c. 200 g) samples collected by GANSSER in 1936. Our much larger samples did not confirm

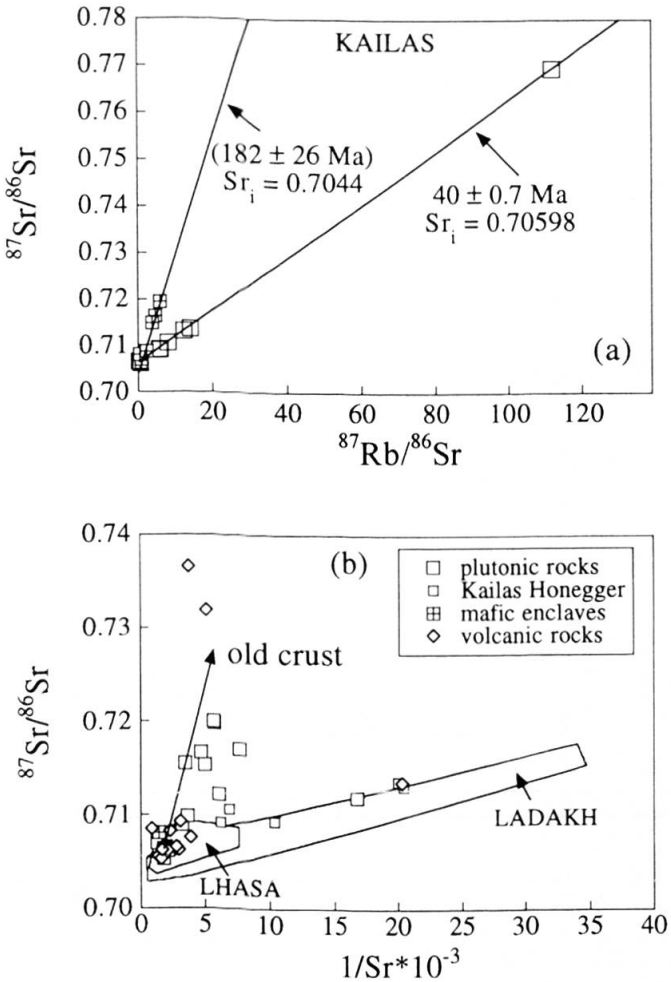

Fig. 5 (a) $^{87}Rb/^{86}Sr$ vs $^{87}Sr/^{86}Sr$ plot for intrusive rocks from the Kailas pluton, THB, SW Tibet, including the 38.8 Ma isochron of HONEGGER et al. (1982). In contrast, the data obtained on eleven larger samples collected in 1993 plot along an errorchron of distinctly older age. The pronounced data scatter suggests incomplete isotope homogenization within the pluton or, alternatively, a heterogeneous intrusion history. (b) $^{87}Sr/^{86}Sr$ vs 1/Sr plots for intrusive rocks from SW Tibet.

Tab. 3 Ar–Ar, Pb–Pb, U–Pb and Rb–Sr ages of plutonic and volcanic rocks from the THB, SW Tibet.

Sample no.	Location	Lithology	Mineral	Pb–Pb; U–Pb (Ma)	Rb–Sr (Ma)	$^{39}Ar/^{40}Ar$ total gas age (Ma)	$^{39}Ar/^{40}Ar$ plateau age (Ma)	plateau steps	plateau % ^{39}Ar	inverse isochron correlation age (Ma)	correlation factor	$^{40}Ar/^{36}Ar$ initial
PLUTONIC ROCKS												
HF197/93	W Kailas	Hb-granodiorite	zircon (2 crystals)	119.3 ± 14.7								
HF197/93	W Kailas	Hb-granodiorite	sphene	107.0 ± 3,0								
HF197/93	W Kailas	Hb-granodiorite	amphibole			43.0 ± 1.4	42.8 ± 1.3	3–9	97	37.7 ± 3.7	0.976	327 ± 37
HF197/93	W Kailas	Hb-granodiorite	biotite			35.2 ± 0.3	34.8 ± 0.4	3–9	88	34.8 ± 1.1	0.714	423 ± 186
HF197/93	W Kailas	Hb-granodiorite	plagioclase			33.1 ± 0.7						
HF197/93	W Kailas	Hb-granodiorite	WR-bio		36.0 ± 0.3							
CM106/93	E Kailas	Hb-granodiorite	sphene	104.0 ± 2.0								
CM108/93	E Kailas	mafic enclave	biotite			39.2 ± 0.7	39.8 ± 0.5	7–15	94	40.0 ± 0.2	0.999	284 ± 8
CM108/93	E Kailas	mafic enclave	WR-bio		39.0 ± 0.4							
HF194/93	NW Kailas	aplitic dikes	WR (3 samples)		40.0 ± 0.7							
CM061/93	S Labru	Hb-gabbro	sphene	109.0 ± 1,0								
TE019/93	SE Xungba	Hb-granite	zircon (4 crystals)	116.2 ± 2.4								
TE019/93	SE Xungba	Hb-granite	biotite			91.5 ± 0.9	92.3 ± 0.8	3–12	98	92.4 ± 0.5	0.999	399 ± 33
TE019/93	SE Xungba	Hb-granite	WR-bio		90.3 ± 0.9							
CM059/93	SW Labru	mylonitic granite	WR – Ms – Pl – Kf		12.1 ± 2.4							
CM068/93	SW Labru	cataclastic granite	orthoclase			31.3 ± 0.4	31.6 ± 0.4	3–14	96			
HF091-095/93	SE Gar	syenite	WR (3 samples)		63.5 ± 4.9							
VOLCANIC ROCKS												
TE028/93	SE Xungba	rhyolite (TF)	sanidine				105.0 ± 2.0	9–12	34			
TE084/93	W Jarga	andesite (TF)	WR-plagioclase		119.5 ± 3.2							
TE084/93	W Jarga	andesite (TF)	plagioclase			93.2 ± 2.9				92.2 ± 2.9	0.889	322 ± 52
TE078/93	W Jarga	rhyolite (LZ)	WR-plag-biotite		51.9 ± 0.4							
TE086/96	SW Jarga	andesite (LZ)	WR-biotite		36.6 ± 2.7							
TE087/93	SW Jarga	dacite (LZ)	sanidine			43.4 ± 1.3	43.4 ± 1.2	6–11	62	44.8 ± 1.1	0.976	279 ± 19
TE114/93	E Jarga	dacite (LZ)	biotite			53.6 ±1.1	54.0 ± 1.0	5–10	81	54.1 ± 0.6	0.966	294 ± 11
TE114/93	E Jarga	dacite (LZ)	plagioclase			50.3 ± 1.0	52.5 ± 0.6	8–10	61			
TE233/93	S Barga	dacite (LZ)	plagioclase			53.0 ± 2.2						
CM028/93	SW Labru	rhyolitic dike	WR-muscovite		36.5 ± 0.2							
CM028/93	SW Labru	rhyolitic dike	muscovite			16.8 ± 0.3	17.0 ± 0.2	3–8	87	17.2 ± 0.3	0.999	259 ± 48

LZ = Linzizong Formation; TF = Takena Formation.

this surprisingly young age. The new data plot along an errorchron of distinctly older age (182 ± 26 Ma; Fig. 5a). The Rb–Sr data on highly evolved cross-cutting aplitic dikes, however, give an age of about 40 Ma (Fig. 5a). Two syenites and a trachytic dike from Gar yielded a Rb–Sr age of 63.5 ± 4.9 Ma (M.S.W.D. = 0.71) with an initial $^{87}Sr/^{86}Sr$ ratio of 0.70358 (Tab. 2).

In order to determine reliable crystallization ages for the THB, zircons from two hornblende-granodiorites were analyzed by the evaporation technique (KLÖTZLI, 1997). The zircon rims from sample TE19/93 (c. 120 km N of Mt. Kailas) yielded an age of 116.2 ± 2.4 Ma. Three of these crystals contain older cores with an age range of 400 to 900 Ma in the high temperature evaporation steps (Tab. 4). Two zircons from sample HF197/93 (Mt. Kailas) yielded ages of 152.5 ± 15.8 Ma and 119.3 ± 14.7 Ma, respectively (Tab. 4). These values are probably due to an inherited lead component and interpreted as maximum ages. An inherited lead component of Precambrian to lower Paleozoic age was also detected in zircons from THB plutons in the Lhasa-Xigaze segment (SCHÄRER et al., 1984b).

In addition, sphene was analyzed by the U–Pb method (Tab. 5). In the Tera-Wasserburg diagram, three sphene fractions from the Kailas granodiorite HF197/93 define a discordia with an upper intercept age of 107.2 ± 1.4 and a lower intercept age of 33.8 ± 7.3 Ma. A single fraction from mafic enclave CM106/93 lies on the same discordia. Regression of all four fractions results in intercept values of 107.3 ± 1.4 Ma and 33 ± 7 Ma (Fig. 6). Two sphene fractions of Hb-gabbro sample CM61/93 define an upper intercept of 108.9 ± 0.4 Ma. The lower intercept is at 2 ± 3 Ma. Both upper intercept ages are interpreted as dating cooling to c. 600–650 °C after pluton emplacement. The lower intercept age of the Kailas samples (HF197/93, CM106/93) provides some evidence for an Oligocene (hydro-) thermal event leading to a slight lead loss in the investigated sphenes. In contrast, the sample from the Labru pluton (CM61/93) does not show a Tertiary overprint. The lower intercept is interpreted a being due to lead loss by recent weathering.

The zircon evaporation ages agree with earlier results for the first phase of plutonism in Ladakh (HONEGGER et al., 1982; SCHÄRER et al., 1984a). U–Pb zircon ages from two Gangdese diorites in the Xigaze area, about 500 km to the E of Kailas, are 93.4 ± 1 Ma and 94.2 ± 1 Ma, respectively (SCHÄRER et al., 1984a).

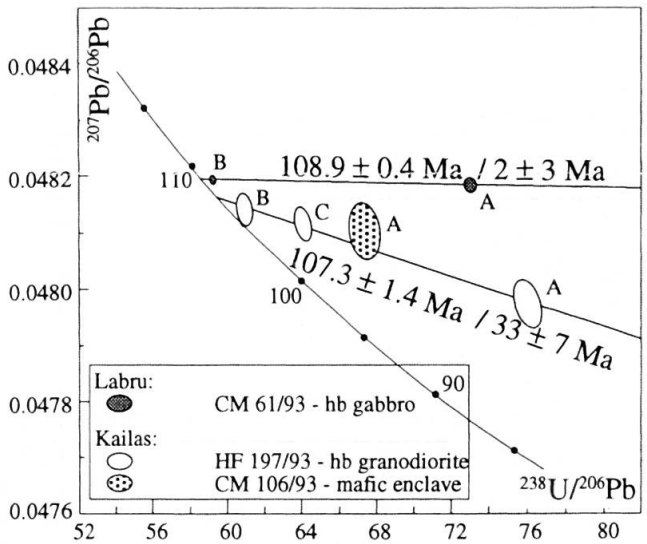

Fig. 6 Concordia diagram for sphenes from hornblende-granodiorite HF197/93 (Kailas), mafic enclave CM108/93 (Kailas) and Hb-gabbro CM61/93 (Labru).

VOLCANIC ROCKS

The $^{40}Ar/^{39}Ar$ and Rb–Sr age data are listed in table 3 and also presented as age spectra (Fig. 7). The andesitic lava TE 84/93 (Takena Formation W of Xungba, Fig. 2) yielded a Rb–Sr age of 119.5 ± 3.2 Ma (Fig. 7a). Its plagioclase $^{40}Ar/^{39}Ar$ spectrum is complex, the total gas age of 93.2 ± 2.9 Ma probably dates hydrothermal alteration (Fig. 7b). Feldspars (sanidine and altered plagioclase) of rhyolite TE 28/93 in the uppermost part of the Takena Formation gave a composite $^{40}Ar/^{39}Ar$ plateau (Fig. 7c): the age of 105 ± 2 Ma in the high-temperature steps probably dates the fresh sanidine and thus the age of extrusion. A later thermal event is indicated by the significantly younger total gas "age" of 91.1 ± 1.9 Ma and the 82.6 ±1.4 Ma plateau.

The ignimbrites associated with the Linzizong Formation in SW Tibet are Eocene in age. The WR-biotite Rb–Sr isochron of rhyolitic ignimbrite TE78/93 (E Jarga) yielded an age of 51.9 ± 0.4 Ma (Fig. 7d). Biotite and plagioclase from dacite sample TE114/93 (E Jarga) yielded $^{40}Ar/^{39}Ar$ plateau ages of 54 ± 1.0 Ma and 52.5 ± 0.6 Ma, respectively (Figs 7 e, f). A Rb–Sr isochron age of 46 ± 4.5 Ma was determined for samples TE105/93 and TE110/93 (S Jarga). A $^{40}Ar/^{39}Ar$ plateau age of 43.4 ± 1.2 Ma has been obtained on sanidine from the subvolcanic dacite TE87/93 (Fig. 7g). Andesite TE86/93 yielded a WR-biotite Rb–Sr age of 36.9 ± 2.7 Ma (Fig. 7h). Near Labru, two-mica rhyolitic dikes (CM28/93; CM60/93) with a Rb–Sr age of 36.5 ± 0.2 Ma (WR-Mus, Tab. 3) crosscut the THB plutonic rocks.

Tab. 4 Single zircon evaporation data for two THB granitoids, SW Tibet.

Sample	No. of blocks	evaporation temperature °C a)	$^{207}Pb/^{206}Pb$ b)	2 SE c)	2 SE % c)	$^{207}Pb/^{206}Pb$ age Ma d)	2 SE Ma b)	2 SE % b)	$^{208}Pb/^{206}Pb$ b)	2 SE b)	Th/U at 7-6 age e)	2 SE b)
TE19/93Ac2	11	1390	0.048226	0.000470	1.0	110.4	23.0	20.9	0.148	0.048	0.458	0.370
TE19/93Ac3	7	1400	0.048224	0.000365	0.8	110.3	17.9	16.2	0.151	0.049	0.467	0.321
TE19/93Ac4	11	1400	0.048421	0.000101	0.2	119.9	4.9	4.1	0.315	0.040	0.975	0.209
TE19/93Ac5	10	1420	0.055550	0.005966	10.7	434.4	240.9	55.5	0.265	0.011	0.803	1.467
TE19/93Ac6	11	1440	0.054759	0.000676	1.2	402.4	27.7	6.9	0.450	0.038	1.367	0.325
TE19/93Ac7	9	1450	0.057562	0.002178	3.8	513.1	83.2	16.2	0.413	0.007	1.246	0.480
TE19/93Ac8	13	1460	0.059584	0.001305	2.2	588.5	47.5	8.1	0.408	0.018	1.225	0.280
TE19/93Ac9	4	1460	0.060349	0.001383	2.3	616.1	49.5	8.0	0.407	0.005	1.220	0.235
TE19/93Ac10	6	1480	0.069357	0.002404	3.5	909.4	71.4	7.9	0.431	0.001	1.269	0.239
mean rim: c2–c4			0.048291	0.000093	0.2	**113.5**	**4.5**	4.0				
TE19/93Bc1	10	1418	0.04850	0.00143	3.0	124	70	56.3	0.172	0.002	0.533	0.915
TE19/93Bc2	16	1490	0.04829	0.00739	15.3	113	220	193.9	0.268	0.084	0.830	1.689
mean			0.048394	0.000106	0.2	**118.6**	**5.2**	4.4				
TE19/93Cc2	10	1416	0.048318	0.011844	24.5	114.8	304.7	265.3	0.202	0.028	0.623	0.704
TE19/93Cc4	12	1438	0.048532	0.000961	2.0	125.3	26.8	21.4	0.302	0.023	0.935	0.511
TE19/93Cc5	7	1459	0.048051	0.000510	1.1	101.7	16.8	16.5	0.292	0.029	0.903	0.409
TE19/93Cc6	9	1493	0.052243	0.002637	5.0	296.0	58.1	19.6	0.544	0.117	1.665	1.123
mean rim: c2–c5			0.048300	0.000197	0.4	**114.0**	**9.6**	8.4				
TE19/93Dc1	11	1420	0.048348	0.006198	12.8	116.3	196.8	169.2	0.304	0.070	0.940	2.246
TE19/93Dc2	1	1420	0.048439	0.000432	0.9	120.8	21.0	17.4	0.037	0.008	0.115	0.070
TE19/93Dc3	13	1460	0.047557	0.008870	18.7	77.3	234.6	303.6	0.175	0.013	0.541	0.475
TE19/93Dc4	15	1460	0.049813	0.001774	3.6	186.3	83.0	44.6	0.097	0.014	0.299	0.414
TE19/93Dc5	4	1500	0.056581	0.000963	1.7	475.2	37.7	7.9	0.098	0.043	0.296	0.192
mean rim: c1–c2			0.048393	0.000046	0.1	**118.5**	**2.2**	1.9				
HF197/93B												
HF197/93Bc1	9	1430	0.048767	0.001188	2.4	136.6	57.3	41.9	0.443	0.040	1.367	1.615
HF197/93Bc2	5	1470	0.049430	0.000801	1.6	168.2	37.9	22.5	0.357	0.023	1.100	0.619
mean			0.049098	0.000331	0.7	**152.5**	**15.8**	10.4				
HF197/93C												
HF197/93Cc1	10	1450	0.048409	0.000301	0.6	**119.3**	**14.7**	12.3	0.248	0.152	0.766	0.692

a) Error on evaporation temperature is estimated to be ± 10 °C.
b) Weighted mean from individual scan ratios.
c) All errors reported are 2 standard errors of the mean.
d) Mean ages derived from individual scan ratios and not from individual scan ages.

Tab. 5 Sphene U–Pb data, THB granitoids, SW Tibet.

Fraction	weight mg	U ppm a	Pb* ppm a	$^{206}Pb/^{204}Pb$ a	Pb ng c	$^{208}Pb/^{206}Pb$	$^{206}Pb/^{238}U$ %	$^{207}Pb/^{235}U$ %	Corr. Coeff.	$^{207}Pb/^{206}Pb$ %	$^{207}Pb/^{206}P$ Age (Ma)
HF197/93											
Fraction A	14.00	135	2.90	53.6	43.61	0.8459	0.013156 ± 0.91	0.08702 ± 8.0	0.6825	0.04798 ± 0.047	98 ± 2
Fraction B	13.57	156	3.77	67.7	43.55	0.6618	0.016424 ± 0.61	0.10902 ± 5.4	0.6493	0.04814 ± 0.050	106 ± 2
Fraction C	14.76	253	5.76	64.7	77.97	0.6398	0.015624 ± 0.65	0.10366 ± 5.6	0.6769	0.04812 ± 0.052	105 ± 2
CM061/93											
Fraction A	32.90	979	25.00	157.0	197.0	1.2137	0.013705 ± 0.35	0.09105 ± 2.6	0.6766	0.04819 ± 0.024	108 ± 1
Fraction B	60.46	267	7.99	191.0	98.56	1.0071	0.016881 ± 0.24	0.11218 ± 1.6	0.6438	0.04819 ± 0.015	109 ± 1
CM106/93											
Fraction A	47.73	273	5.25	52.8	346.0	0.9966	0.014847 ± 1.0	0.09849 ± 9.1	0.7191	0.04810 ± 0.084	104 ± 2

Errors are 1 std. error of mean in % except 207/206 age errors which are 2 std. errors in Ma; * = radiogenic Pb, a = include sample weight error of ± 0.01 mg in concentration uncertainty; c = total common Pb in analysis.

Igneous petrogenesis

Calc-alkaline magmatic rocks – The THB plutonic and volcanic rocks in southern Tibet display a wide range in an εNd vs initial $^{87}Sr/^{86}Sr$ diagram (Fig. 4). This rules out an origin by fractionation of a common parental magma. In addition, the absence of a correlation for $^{87}Sr/^{86}Sr$ vs 1/Sr (Fig. 5b) rules out an origin by simple mixing processes. This is also seen in figure 4, where bulk mixing between asthenospheric melts and the 531 Ma Amdo orthogneiss, the only known basement sample of the Lhasa block (HARRIS et al., 1988), cannot generate the observed isotopic variation. The Sr isotopes (< 0.705) of many Hb-granitoids from SW Tibet indicate that they are essentially mantle-derived, with some input of continental crust. In contrast, Bio-granites and leucogranites have $^{87}Sr/^{86}Sr$ initial ratios > 0.708 that indicate a considerable crustal influence.

Although a genetic link between the hornblende granitoids and gabbros is suggested by their close association in space and time and by similar Sr and Nd isotope ratios, the mafic rocks do not provide satisfactory parental melt compositions. Their non-primitive *mg*-numbers (48–58) and the low Cr and Ni values suggest significant olivine ± pyroxene fractionation. Their lack of Eu anomalies argues against significant plagioclase fractionation and indicates that the source was plagioclase-free and therefore located in the mantle. Although the trace element signature of the analyzed gabbros and basalts (Fig. 3b) are typical of subduction-related volcanics (high Ba/La, Th/Yb and Sr/Nd, and low Nb/La and Ta/Yb ratios), data are insufficient to constrain source components, contaminants and the proportions of mixing among various source components or among variably evolved magma batches. In any case, an input of mafic melts from the mantle could have provided heat for crustal melting and granitoid genesis (e. g. HUPPERT and SPARKS, 1988).

Syenites – The Gar syenitic and trachytic rocks have Y/Nb ratios of less than 1.2, low initial Sr (0.70358) ratios and positive initial εNd values. According to EBY (1992) this would permit an origin as differentiates from basaltic magmas derived from an enriched mantle source. Negative Ta–Nb-anomalies (Fig. 3c), however, are not observed in rift- or hotspot-related trachytes and syenites, and could indicate that the parental magma was related to a subduction-modified mantle source, although extensive crystal fractionation cannot be discounted.

It is commonly assumed that alkaline magmatism is favoured by extensional tectonics and that A-type granitoids are emplaced into late- to post-orogenic settings. The Rb–Sr age data, however, suggest that the Gar syenites were emplaced into an active collisional environment. Other examples of alkaline pre-collisional plutonism in the India-Eurasia collision zone include the late Cretaceous A-type granitoids from the Karakoram batholith (DEBON and KHAN, 1996) and from the Indus suture zone near Kargil (BROOKFIELD and REYNOLDS, 1981). Only the Hemasil syenites were intruded in late Miocene times (LEMENNICIER et al., 1996).

Cooling and exhumation history

Our data indicate that the Kailas pluton experienced a longer lasting period of magmatic activity, cooling and exhumation than previously considered. The Kailas granodiorite HF197/93 intruded around 120 Ma ago. The time for cooling from c. 800 °C to c. 650 °C, based on the difference in closure temperature for Pb in zircon and in sphene, is c. 12 Ma. The $^{40}Ar/^{39}Ar$ release spectrum for amphibole from the Kailas granodiorite HF197/93 indicates cooling to c. 500 °C at 42.8 ± 1.3 Ma (Fig. 8a). Biotite and plagioclase separates from the same sample yielded $^{40}Ar/^{39}Ar$ ages of 35.2 ± 0.3 Ma and 33.1 ± 0.7 Ma, respectively (Figs 8 b, c and Tab. 3). Hence the cooling path for this sample must have been characterized by an average cooling rate of c. 4 °C/Ma until about 43 Ma, followed by a period of a distinctly accelerated cooling rate (Fig. 9). YIN et al. (1996) also reported a hornblende cooling age of 45 ± 2 Ma from the Kailas pluton and a rapid cooling episode shown by the K-feldspar spectrum between 30 and 25 Ma, based on $^{40}Ar/^{39}Ar$ thermochronometry. This suggests that the plutonic belt was not thickening and isostatically adjusting elevation to a significant extent before the late Oligocene, followed by a profound change in unroofing rate. Exhumation and unroofing must have been completed before about 23 Ma, the time of deposition of the Kailas Molasse (SCHUSTER et al., 1997).

The exhumation and cooling history for the hornblende-granodiorite TE19/93 in the northern part of the THB was distinctly different. Following crystallization at about 116 Ma (Tab. 3), cooling at an average rate of c. 15 °C/Ma is indicated by the $^{40}Ar/^{39}Ar$ biotite age of 92.3 ± 0.8 Ma (Tab. 3, Figs 8 g, h). The timing of exhumation and erosion is unknown, but must have occurred quite early because Eocene volcanic rocks of the Linzizong Fm. and post-collisional ultrapotassic lavas that extruded between 26 and 17 Ma rest unconformably on top of this granite (MILLER et al., 1999).

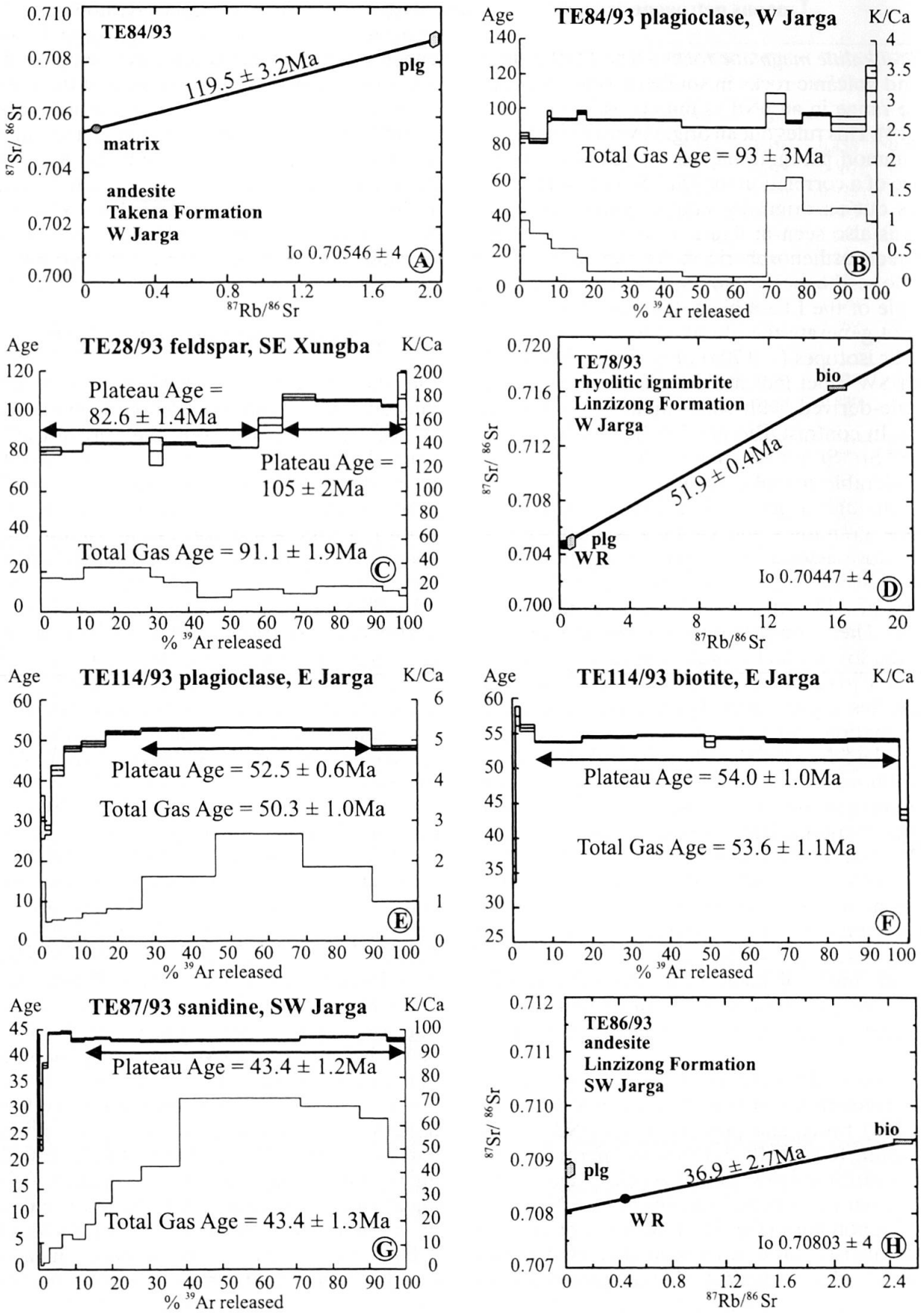

Fig. 7 $^{40}Ar/^{39}Ar$ and Rb/Sr age data of volcanic rocks from the Takena and Linzizong formations, SW Tibet: andesite TE84/93 (a, b), rhyolite TE28/93 (c), ignimbrite TE78/93 (d), andesite TE114/93 (e, f), dacite TE87/93 (g), andesite TE86/93 (f). The quoted Ar ages are integrated over release fractions underlined by the arrow and discussed in the text.

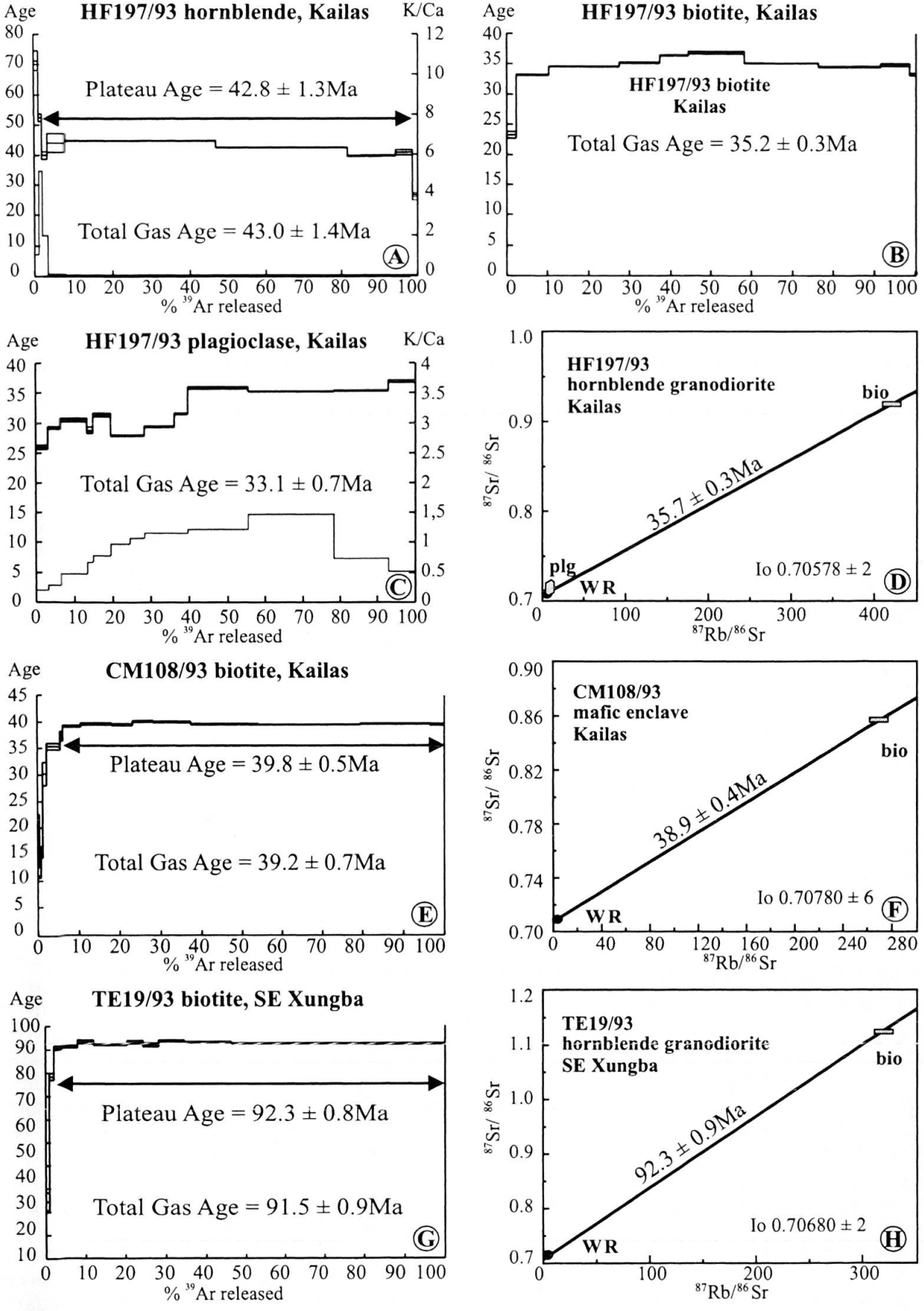

Fig. 8 $^{40}Ar/^{39}Ar$ and Rb/Sr age data of THB plutonic rocks from SW Tibet: hornblende-granodiorite HF197/93 (a–d); mafic enclave CM108/93 (e, f); hornblende-granodiorite TE19/93 (g, h). The quoted Ar ages are integrated over release fractions underlined by the arrow and discussed in the text.

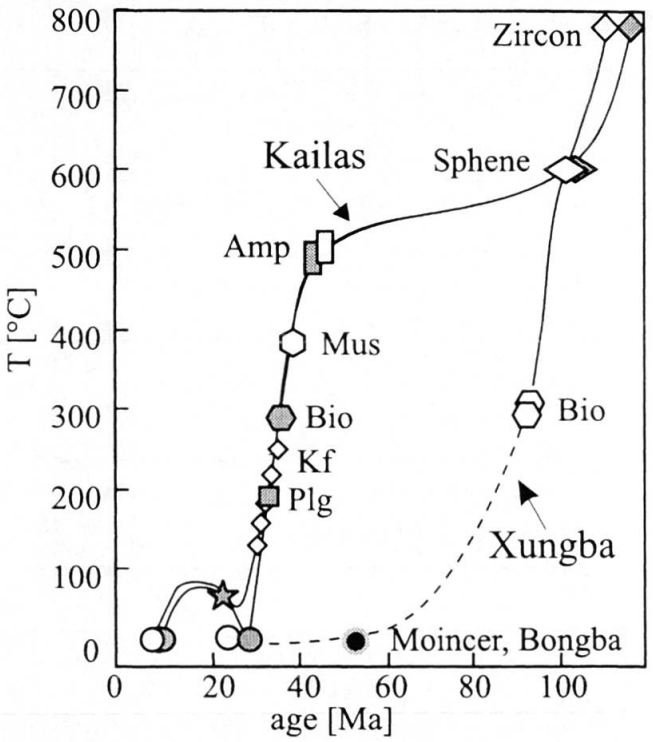

Fig. 9 Temperature-time paths for THB granodiorites in SW Tibet based on radiometric mineral formation and cooling ages, showing different exhumation and erosion histories for plutons in the northern and southern parts of the batholith. Large filled symbols: HF 197/93 (Kailas, southern part of the THB). Asterisk: vitrinite reflectance measured on coals within the Kailas Molasse, documenting post-depositional burial diagenesis and geothermal activity. Small open diamonds: Kailas, $^{40}Ar/^{39}Ar$ data from YIN et al. (1999). Large open symbols: granodiorite TE019/93 (SE Xungba, northern part of the THB). Near Bongba (Fig. 2) the plutonic rocks are overlain by the Linzizong Formation. North of Moincer, the THB is transgressed by the Eocene Moincer Formation.

Previous work (PAN et al., 1993; COPELAND et al., 1995) has revealed that several plutons of the Gangdese batholith in the Lhasa area have experienced pulses of rapid cooling at various times after the collision. According to HARRISON et al. (1992) rapid denudation of the Gangdese batholith is due to motion on the Gangdese thrust, a major N-dipping thrust system with a top-to-the-south sense of shear that cuts and brings Gangdese plutonic rocks over Xigaze forearc sediments and Tethyan sedimentary rocks of the Indian plate. A mechanism similar to that proposed by YIN et al (1999) could have operated in SW Tibet. Our data support their three-stage kinematic model, but extend the tectonomagmatic to 120 Ma (Stage 0).

Stage 0 started with the intrusion of plutons and associated volcanic activity. However, the cooling history of the northern parts of the THB is distinctly different from that of the southern Kailas area. This observation cannot be simply explained by tilting and block rotation of the THB, but suggests different exhumation histories and thus south-directed thrusting tectonics predating the Gangdese thrust (Stage 1 and 2 of YIN et al., 1999). Although such thrusts have been mapped (between Gegar and Jarga, Fig. 2), structural field observations and geochronological data are insufficient to determine location and timing of movement. In addition, Stages 1–3 may have deformed this older thrust system and account for the fact that the southern plutons north of Moincer are also transgressed by the Eocene, whereas the Kailas pluton just 50 km east of Moincer must still have been at mid-crustal levels as documented by the $^{40}Ar/^{39}Ar$ hornblende cooling age of 43 Ma. The rapid cooling and exhumation to the surface before 23 Ma (SCHUSTER et al., 1997) probably reflects the position of the hanging wall above the south-directed Gangdese thrust as suggested by Stages 1 and 2 of YIN et al. (1999). The short period of reheating of these rocks after 23 Ma (Stage 3) supports the model of a footwall position below the north-directed Kailas thrust (YIN et al., 1999).

Tectonomagmatic model

This study revises the only published age for the Kailas plutonic rocks and presents new data on the age of crystallization and cooling for plutonic and volcanic rocks in SW Tibet. Table 6 lists these and published geochronologic data related to the crystallization of pre- and post-collision magmatic rocks from different sectors of the Transhimalaya magmatic belt, showing that in SW Tibet the predominantly calc-alkaline plutonic activity started around 120 Ma and continued at least with minor felsic intrusions until about 40 Ma. In addition, our data show that the calc-alkaline volcanism in SW Tibet also spanned middle Cretaceous to Eocene time, indicating that the continental margin magmatism did not end synchronously with initial collision at c. 60–50 Ma (e. g. KLOOTWJIK et al., 1985; 1992). A similar time span for subduction-related plutonic and volcanic activity has been reported from Pakistan (e. g. PETTERSON and WINDLEY, 1985), Ladakh (HONEGGER et al., 1982; SCHÄRER et al., 1984a) and south central Tibet (SCHÄRER et al., 1984b; DEBON et al., 1986). It is interesting to note that U–Pb data on plutonic rocks from the Transhimalaya magmatic belt (Tab. 6), define two major intervals of calc-alkaline magmatism: one during the middle Creta-

Tab. 6 New and published age data of magmatic rocks from different parts of the Transhimalaya magmatic belt.

Location	Rock type		Method		Age (Ma)	T_{DM}Nd (Ga)	Reference
SW Tibet							
Kailas	granodiorite	Transhimalaya batholith	U–Pb	zircon	119.3 ± 14.7	0.78	this work
S Xungba	granodiorite	Transhimalaya batholith	U–Pb	zircon	116.2 ± 2.4	0.80	this work
SE Gar	syenites	Transhimalaya batholith	Rb–Sr	WR	63.5 ± 4.9	0.60	this work
Kailas	aplitic dikes	Transhimalaya batholith	Rb–Sr	WR	40.0 ± 0.7		this work
Kailas	P + V	Transhimalaya batholith	Rb–Sr	WR	38.8 ± 1.3		HONEGGER et al., 1982
Labru	rhyolite dike	Transhimalaya batholith	Rb–Sr	WR-Ms	36.5 ± 0.2		this work
W Jarga	andesite	Takena Fm.	Rb–Sr	WR-Plg	119.5 ± 3.2	0.60	this work
S Xungba	rhyolite	Takena Fm.	$^{40}Ar/^{39}Ar$	San	104.4 ± 2.7		this work
W Jarga	andesite	Takena Fm.	$^{40}Ar/^{39}Ar$	Plg	93.2 ± 2.9		this work
E Jarga	dacite	Linzizong Fm.	$^{40}Ar/^{39}Ar$	Bio	54.6 ± 1.0	0.90	this work
N Kailas	dacite	Linzizong Fm.	$^{40}Ar/^{39}Ar$	Plg	37.7 ± 3.5		this work
S Tibet							
Dagzhuka	diorite	Gangdese batholith	U–Pb	zircon	94.2 ± 1.0		SCHÄRER et al., 1984a
Dagzhuka	diorite	Gangdese batholith	U–Pb	zircon	93.4 ± 1.0		SCHÄRER et al., 1984a
Quxu	granodiorite	Gangdese batholith	U–Pb	zircon	41.7 ± 0.4		SCHÄRER et al., 1984a
Quxu	granodiorite	Gangdese batholith	U–Pb	zircon	41.1 ± 0.4	0.31	SCHÄRER et al., 1984a; HARRIS et al., 1988
Lhasa	granodiorite	Gangdese batholith	U–Pb	zircon	c. 53		SCHÄRER et al., 1984a
Lingzhu	andesite	Takena Fm.	$^{40}Ar/^{39}Ar$	Amp	90.0 ± 2		COULON et al., 1986
Yangbajain	ignimbrite	Linzizong Fm.	Rb–Sr	WR-Bio	56.2 ± 1.4		XU et al., 1985
Lingzhu	andesite	Linzizong Fm.	$^{40}Ar/^{39}Ar$	Bio	59.0 ± 2		COULON et al., 1986
Lingzhu	andesite	Linzizong Fm.	$^{40}Ar/^{39}Ar$	Plg	49.2 ± 1		COULON et al., 1986
NW India							
Ladakh	granodiorite	Ladakh-arc batholith	U–Pb	zircon	101 ± 2.0	0.71	SCHÄRER et al., 1984b; ALLÈGRE and BEN OTHMAN, 1980
Ladakh	granite	Ladakh-arc batholith	U–Pb	zircon	c. 60		SCHÄRER et al., 1984b
Kargil	granodiorite	Ladakh-arc batholith	U–Pb	zircon	103.0 ± 3.0		HONEGGER et al., 1982
Shey	granite	Ladakh-arc batholith	Rb–Sr	WR	60.3 ± 10		HONEGGER et al., 1982
Ladakh	granite	Ladakh-arc batholith	U–Pb	zircon	c. 59		WEINBERG, 1997
Leh	granodiorite	Ladakh-arc batholith	U–Pb	zircon	c. 50		WEINBERG, 1997
Kargil	syenite	Indus suture zone	$^{40}Ar/^{39}Ar$	Amp	82.0 ± 6		BROOKFIELD and REYNOLDS, 1981
Pakistan							
K2	granodiorite	Karakoram batholith	U–Pb	zircon	c. 115–120		SEARLE et al., 1991
Hunza	granodiorite	Karakoram batholith	U–Pb	zircon	95.0 ± 5		LEFORT et al., 1983
Batura	granites	Karakoram batholith	Rb–Sr	WR	43.0 ± 3		DEBON et al., 1987
Baltoro	granite	Karakoram batholith	U–Pb	zircon	21.5 ± 0.5		PARRISCH and TIRRUL, 1989
Matum Das	tonalite	Kohistan-arc batholith	Rb–Sr	WR	102.0 ± 12		PETTERSON and WINDLEY, 1985
Dainyar	diorite	Kohistan-arc batholith	$^{40}Ar/^{39}Ar$	Amp	54.0 ± 1		TRELOAR et al., 1989
Gilgit	granite	Kohistan-arc batholith	Rb–Sr	WR	54.0 ± 4		PETTERSON and WINDLEY, 1985
Shirot	granite	Kohistan-arc batholith	Rb–Sr	WR	40.0 ± 6		PETTERSON and WINDLEY, 1985
Indus confl.	leucogranites	Kohistan	Rb–Sr	WR	34.0 ± 14		PETTERSON and WINDLEY, 1985
Parri	leucogranites	Kohistan	Rb–Sr	WR	29.0 ± 8		PETTERSON and WINDLEY, 1985
Gakuch	basalt	Kohistan	$^{40}Ar/^{39}Ar$	Amp	61.0 ± 2		TRELOAR et al., 1989
Phandar	basalt	Kohistan	$^{40}Ar/^{39}Ar$	Amp	58.0 ± 2		TRELOAR et al., 1989

ceous, c. 120–90 Ma, and one during the Paleocene and Eocene, c. 60–40 Ma. According to GLAZNER (1991) major episodes of arc-related plutonism correlate with periods of oblique subduction, whereas arc-nomal contraction facilitates fracture transport of magmas to the surface and volcanism. Geochronological as well as structural data are still too sparse to really test a possible tie between oblique convergence and batholith emplacement within the Transhimalaya magmatic arc. More-

over, the available data for the different sectors indicate that plutonic and volcanic rocks are roughly coeval.

The Gar alkaline magmatic complex is a part of the Transhimalaya batholith. Its emplacement at c. 64 Ma coincided with the beginning of collision. The oblique collision of India and Eurasia and decreasing rates of convergence should have resulted in complex tectonic features, including transtensional tectonics and local extension that may have helped these magmas to ascend. According to the mechanism proposed by McCAFFREY and NABELEK (1998), extension in the upper plate results from basal shear caused by the Indian lithosphere sliding obliquely beneath Tibet along an arcuate plate boundary. This mechanism may have helped magmas to ascend during several tens of Ma before, during and after collision of the Indian and Asian continental plates.

As table 6 shows, magmatism did not end in the late Eocene. Post-collisional granites occur along the strike of the THB, but only in the Karakoram batholith do voluminous plutons such as the Miocene Baltoro unit indicate large-scale crustal melting (e. g. SEARLE, 1991). In SW Tibet, the Oligocene dacitic and rhyolitic dikes near Labru are peraluminous and characterized by $^{87}Sr/^{86}Sr$ initial ratios in the range 0.708–0.736 (Tab. 2). They could represent crustally derived melts, similar to those that produced the Oligocene two-mica leucogranitic dike swarms in Kohistan (PETTERSON and WINDLEY, 1985) and the garnet-bearing leucogranites in Ladakh (RAZ and HONEGGER, 1989).

Conclusions

(i) Hb-granitoids from the THB in SW Tibet (Kailas transect) record equilibration conditions between 700–780 °C, at depths between 9.8–23.6 km. (ii) Calc-alkaline plutonism started as early as 119 Ma and lasted until about 40 Ma. Associated volcanic rocks yielded eruption ages between 120 and 37 Ma. (iii) Distinctly different cooling and exhumation histories of different parts of the THB between 120 and 50 Ma suggest early thrust tectonics (i. e. Stage 0). (iv) The postcrystallization history of the Kailas pluton supports the model of YIN et al. (1999) and is characterized by cooling to below 500 °C and exhumation to the surface between 43–23 Ma, probably due to south directed thrusting along the Gangdese thrust (Stages 1 and 2). Reheating around 20 Ma documents the activity of the north directed South Kailas Thrust system (Stage 3).

Acknowledgements

Samples were collected during the 1993 field trip financed by the Fonds zur Förderung der wissenschaftlichen Forschung (FWF, P9420-GEO), and coordinated in cooperation with the Chengdu College of Geology and the Bureau of Geology and Mineral Resources of Xizang (China). V. Mair and F. Purtscheller took part in the field studies. We thank Liu Jianming (Chinese Research Center of Mineral Resource Exploration, CAS, Beijing) and Xiang Zhou (Bureau of Geology and Mineral Resources, Lhasa) for their support in the field. The critical comments of two anonymous reviewers are gratefully acknowledged.

Appendix

ANALYTICAL TECHNIQUES

The six sphene fractions were handpicked for analysis and washed in diluted high-purity HNO_3 and water prior to chemistry. Sphene dissolution and chemical separation were performed using a slightly modified HCl–HBr ion-exchange chemistry of PARRISH et al. (1992). Total procedural blanks for U and Pb were in the range of 3 pg and 40 pg, respectively. U and Pb concentrations were determined using a ^{233}U–^{235}U–^{205}Pb mixed spike. U and Pb ratios were measured on a Finnigan MAT 262 multicollector mass spectrometer. Corrections for U mass fractionation effects were based on correction factors derived from multiple U500 U standard measurements. Corrections for Pb mass fractionation effects were based on correction factors derived from multiple NBS 982 and NBS 983 standard measurements. Corrections are in the range of 0.09 %/amu for U and 0.12 %/amu for Pb, respectively. Data reduction was done according to PARRISH et al. (1987) and using the software package "isoplot" of LUDWIG (1992).

Single zircon evaporation dating followed modified procedures originally described by KOBER (1987). Full details of the technique applied are summarized in KLÖTZLI (1997). Reported ages and errors are propagated weighted mean values calculated from at least 20 measured $^{207}Pb/^{206}Pb$ ratios. All errors reported are 2 standard errors of the mean (approx. 95% confidence limit). Other analytical methods are given in MILLER et al. (1999). The following model parameters were used for the calculation of depleted mantle (DM) model ages: $^{147}Sm/^{144}Nd = 0.222$, $^{143}Nd/^{144}Nd = 0.513114$ (MICHARD et al., 1985). A linear evolution of the Nd isotope composition of the DM is assumed throughout geological time, εNd values are calculated relative to CHUR.

References

ALLÈGRE, C.J. and BEN OTHMAN, D. (1980): Nd–Sr isotopic relationship in granitoid rocks and continental crustal development: a chemical approach to orogenesis. Nature, 286, 335–341.

BECK, R.A., BURBANK, D.W., SERCOMBE, W.J., RILEY, G.W., BARNDT, J.K., BERRY, J.R., AFZAL, J., KHAN, A.M., JURGEN, H., METJE, J., CHEEMA, A., SHAFIQUE, N.A., LAWRENCE, R.D. and KHAN, M.A. (1995): Stratigraphic evidence for an early collision between northwest India and Asia. Nature, 373, 55–57.

BLUNDY, J.D. and HOLLAND, T.J.B. (1990): Calcic amphibole equilibria and a new amphibole-plagioclase geothermometer. Contrib. Mineral. Petrol., 104, 208–224.

BROOKFIELD, M.E. and REYNOLDS, P.H. (1981): Late Cretaceous emplacement of the Indus suture zone ophiolitic mélanges and an Eocene-Oligocene magmatic arc on the northern edge of the Indian plate. Earth Planet. Sci. Lett., 55, 157–162.

BURG, J.B., PROUST, F., TAPPONNIER, P. and CHEN, G.M. (1983): Deformation phases and tectonic evolution of the Lhasa block (southern Tibet, China). Eclogae geol. Helv., 76, 643–665.

COPELAND, P., HARRISON, T.M., PAN, Y., KIDD, W.S.F., RODEN, M. and ZHANG, Y. (1995): Thermal evolution of the Gangdese batholith, southern Tibet: a history of episodic unroofing. Tectonics, 14, 223–236.

COULON, C., MALUSKI, H., BOLLINGER, C. and WANG, S. (1986): Mesozoic and Cenozoic volcanic rocks from central and southern Tibet: ^{39}Ar–^{40}Ar dating, petrological characteristics and geodynamical significance. Earth Planet. Sci. Lett., 79, 281–302.

CRAWFORD, M.B. and SEARLE, M.P. (1992): Field relationships and geochemistry of pre-collisional (India-Asia) granitoid magmatism in the central Karakoram, northern Pakistan. Tectonophysics, 206, 171–192.

DEBON, F., LE FORT, P., SHEPPARD, S.M.F. and SONET, J. (1986): The four plutonic belts of the Transhimalaya-Himalaya: a chemical, mineralogical, isotopic and chronological synthesis along a Tibet–Nepal section. J. Petrol., 27, 219–250.

DEBON, F., LE FORT, P., DAUTEL, D., SONET, J. and ZIMMERMANN, J.L. (1987): Granites of the western Karakorum and northern Kohistan (Pakistan): a composite mid-Cretaceous to upper Cenozoic magmatism. Lithos, 20, 19–40.

DEBON, F and KHAN, N.A. (1996): Alkaline orogenic plutonism in the Karakorum batholith: the Upper Cretaceous Koz Sar complex (Karambar valley, N. Pakistan). Geodyn. Acta, 9, 145–160.

DEWEY, J., SHACKLETON, R.M., CHANG, C. and SUN, Y. (1988): The tectonic evolution of the Tibetan plateau. Phil. Trans. Royal Soc. London, A327, 379–413.

EBY, G.N. (1992): Chemical subdivision of the A-type granitoids: petrogenetic and tectonic implications. Geology, 20, 641–644.

GANSSER, A. (1964): Geology of the Himalayas. Interscience Publishers, John Wiley and Sons, London, 289 pp.

GLAZNER, A.F. (1991): Plutonism, oblique subduction, and continental growth: An example from the Mesozoic of California. Geology, 19, 984–786.

GILL, J.B. (1981): Orogenic andesites and plate tectonics. Springer-Verlag, Berlin Heidelberg New York, 390 pp.

HARRIS, N.B. W., XU, R., LEWIS, C.L., HAWKESWORTH, C.J. and ZHANG, Y. (1988): Isotope geochemistry of the 1985 Tibet geotraverse, Lhasa to Golmud. Phil. Trans. Royal Soc. London, A327, 263–285.

HARRISON, T.M., COPELAND, P., KIDD, W.S.F. and YIN, A. (1992): Raising Tibet. Science, 255, 1663–1670.

HEIM, A. and GANSSER, A. (1939): Central Himalaya, geological observations of the Swiss expedition 1936. Mem. Soc. Helv. Sci. Nat., 73, 1–245.

HONEGGER, K., DIETRICH, V., FRANK, W., GANSSER, A., THÖNI, M. and TROMMSDORFF, V. (1982): Magmatism and metamorphism in the Ladakh Himalayas (the Indus-Tsangpo suture zone). Earth Planet. Sci. Lett., 60, 253–292.

HUPPERT, H.E. and SPARKS, R.S.J. (1988): The generation of granitic magmas by intrusion of basalt into continental crust. J. Petrol., 29, 599–624.

KLOOTWIJK, C.T., CONAGHAN, P.J. and POWELL, C.M. (1985): The Himalayan Arc: large-scale continental subduction, oroclinal bending and back-arc spreading. Earth Planet. Sci. Lett., 75, 167–183.

KLOOTWIJK, C.T., GEE, J.S., PEIRCE, J.W., SMITH, G.M. and MCFADDEN, P.L. (1992): An early India-Asia contact: Paleomagnetic constraints from Ninetyeast Ridge, ODP leg 121. Geology, 5, 395–398.

KLÖTZLI, U.S. (1997): Zircon evaporation TIMS: Method and procedures. The Analyst, 122, 1239–1248.

KOBER, B. (1987): Single-zircon evaporation combined with Pb^+ emitter bedding for $^{207}Pb/^{206}Pb$-age investigations using thermal ion mass spectrometry, and applications to zirconology. Contrib. Mineral. Petrol., 96, 63–71.

LEAKE, B.E. (1978): Nomenclature of amphiboles. Mineral. Mag., 42, 533–563.

LE FORT, P., MICHARD, A., SONET, J. and ZIMMERMANN, J.L. (1983): Petrography, geochemistry and geochronology of some samples from the Karakorum axial batholith (N. Pakistan). In: SHAMS, F.A. (ed.): Granites of Himalayas, Karakorum and Hindu Kush. Punjab Univ., Lahore, 377–387.

LEMENNICIER, Y., LE FORT, P., PÊCHER, A., LAPIERRE, H. and ROLFO, F. (1996): The Hemasil syenitic dome: an example of Miocene syn-orogenic alkaline magmatism (Karakorum – N. Pakistan). Abstract Vol. 11th Himalaya-Karakoram-Tibet Internat. Workshop 1996 (Tucson, USA), 85–86.

LUDWIG, K.R. (1992): Isoplot: A plotting and regression program for radiogenic-isotope data, version 2.57. US Geol. Survey, Open-file report, 91–445.

MCCAFFREY, R. and NABELEK, J. (1998): Role of oblique convergence in the active deformation of the Himalayas and southern Tibet plateau. Geology, 26, 691–694.

MICHARD, A., GURRIET, P., SOUDANT, M. and ALBARÈDE, F. (1985): Nd isotopes in French Phanerozoic shales: external vs internal aspects of crustal evolution. Geochim. Cosmochim. Acta, 49, 601–610.

MILLER, C., SCHUSTER, R., KLÖTZLI, U., FRANK, W. and PURTSCHELLER, F. (1999): Post-collisional potassic and ultrapotassic magmatism in SW Tibet: Geochemical and Sr–Nd–Pb–O isotopic constraints for mantle source characteristics and petrogenesis. J. Petrol., 40, 1399–1424.

PAN, Y., COPELAND, P., RODEN, M.K., KIDD, W.S. and HARRISON, T.M. (1993): Thermal and unroofing history of the Lhasa area, southern Tibet – evidence from apatite fission track thermochronology. Nucl. Tracks Radiat. Meas., 21, 543–554.

PARRISH, R.R., RODDICK, W.D., LOVERIDGE, R.W. and SULLIVAN, R.W. (1987): Uranium-lead analytical techniques at the geochronology laboratory, Geo-

logical Survey of Canada. Geol. Survey Canada Paper 87-2, 3–7.

PARRISH, R.R. and TIRRUL, R. (1989): U–Pb age of the Baltoro granite, northwest Himalaya, and implications for zircon inheritance and monazite U–Pb systematics. Geology, 17, 1076–1079.

PARRISH, R.R., BELLERIVE, D. and SULLIVAN, R.W. (1992): U–Pb chemical procedures for titanite and allanite in the geochronology laboratory, Geological Survey of Canada. Geol. Survey Canada Paper 91-2, 187–190.

PEARCE, J.A., HARRIS, N.B.W. and TINDLE, A.G. (1984): Trace element discrimination diagrams for the tectonic interpretation of granitic rocks. J. Petrol., 25, 956–983.

PETTERSON, M.G. and WINDLEY, B.F. (1985): Rb–Sr dating of the Kohistan arc batholith in the Trans-Himalaya of north Pakistan, and tectonic implications. Earth Planet. Sci. Lett., 74, 45–57.

PETTERSON, M.G. and WINDLEY, B.F. (1991): Changing source regions of magmas and crustal growth in the Transhimalayas: evidence from the Chalt volcanics and Kohistan batholith, Kohistan, northern Pakistan. Earth Planet. Sci. Lett., 102, 326–341.

PUPIN, J.P. and TURCO, G. (1972): Une typologie originale du zircon accessoire. Bull. Soc. Fr. Minéral. Cristallogr., 95, 348–359.

RAZ, U. and HONEGGER, K. (1989): Magmatic and tectonic evolution of the Ladakh Block from field studies. Tectonophysics, 161, 107–118.

SCHÄRER, U., HAMET, J. and ALLÈGRE, C.J. (1984a): The Transhimalaya (Gangdese) plutonism in the Ladakh region: a U–Pb and Rb–Sr study. Earth Planet. Sci. Lett., 67, 327–339.

SCHÄRER, U., XU, R.H. and ALLÈGRE, C.J. (1984b): U–Pb geochronology of Gangdese (Transhimalaya) plutonism in the Lhasa-Xigaze region, Tibet. Earth Planet. Sci. Lett., 69, 311–320.

SCHMIDT, M.W. (1992): Amphibole composition in tonalite as a function of pressure: an experimental calibration of the Al-in hornblende-barometer. Contrib. Mineral. Petrol., 110, 304–310.

SCHUSTER, R., MILLER, CH., PURTSCHELLER, F., FRANK, W. and MAIR, V. (1997): Cross-section through the western Lhasa Block, SW-Tibet. Abstract Vol. 12th Himalaya-Karakoram-Tibet Internat. Workshop 1997 (Rome, Italy), 207–208.

SEARLE, M.P. (1991): Geology and tectonics of the Karakoram mountains. John Wiley & Sons Ltd, Chichester, 169–198.

SUN, S.S. and MCDONOUGH, W.F. (1989): Chemical and isotopic systematics of oceanic basalts: implications for mantle composition and processes. In: SAUNDERS, A.D. and NORRY, M.J. (eds): Magmatism in the Ocean Basins. Geol. Soc. Spec. Publ., 42, 313–345.

TRELOAR, P.J., REX, D.C., GUISE, P.G., COWARD, M.P., SEARLE, M.P., WINDLEY, B.F., PETTERSON, M.G., JAN, M.Q. and LUFF, I.W. (1989): K–Ar and Ar–Ar geochronology of the Himalayan collision in NW Pakistan: constraints on the timing of suturing, deformation, metamorphism and uplift. Tectonics, 8, 881–909.

TULLOCH, A.J. (1976): Comment on "Implications of magmatic epidote-bearing plutons on crustal evolution in the accreted terranes of northwestern North America" and "Magmatic epidote and its petrologic significance". Geology, 14, 186–187.

WATSON, E.B. and HARRISON, T.M. (1983): Zircon saturation revisited: temperature and composition effects in a variety of crustal magma types. Earth Planet. Sci. Lett., 64, 295–304.

WEINBERG, R.F. (1997): SHRIMP age determinations of zircons from Ladakh and Karakoram (Indian Himalayas). Abstract Vol. 12th Himalaya-Karakoram-Tibet Internat. Workshop 1997 (Rome, Italy), 107.

WHALEN, J.B., CURRIE, K.L. and CHAPPELL, B.W. (1987): A-type granites: geochemical characteristics, discrimination and petrogenesis. Contrib. Mineral. Petrol., 95, 407–419.

XU, R.H., SCHÄRER, U. and ALLÈGRE, C.J. (1985): Magmatism and metamorphism in the Lhasa block (Tibet): a geochronological study. J. Geol., 93, 41–57.

YIN, A., MURPHY, M.A., HARRISON, T.M., RYERSON, F.J., ZHENGLE, C., FENG, W.X. and QIANG, Z.X. (1996): Miocene evolution of the Kailas thrust and Gurla Mandhata detachment fault, western Tibet: implications for the displacement history of the Karakorum fault system. Abstract Vol. 11th Himalaya-Karakoram-Tibet Internat. Workshop, Flagstaff (Arizona), 173–174.

YIN, A., HARRISON, T.M., MURPHY, M.A., GROVE, M., NIE, S., RYERSON, F.J., FENG, W.X. and LE, C.Z. (1999): Tertiary deformation history of southeastern and southwestern Tibet during the Indo-Asian collision. Geol. Soc. Amer. Bull., 111, 1644–1664.

Manuscript received June 11, 1999; revision accepted January 6, 2000.